Materials Advances

ROYAL SOCIETY OF CHEMISTRY

REVIEW

View Article Online
View Journal | View Issue



Cite this: *Mater. Adv.*, 2025, **6**, 6664

# Metal oxide doped organic thin film transistors: a comprehensive review

Nikhil Pais, Manav Jeetendra Shirodkar and Poornima Bhagavath *

In recent years, organic thin film transistors (OTFTs) have been gaining widespread interest for electronic displays, circuits and sensors over traditional silicon-based transistors due to their unique properties such as low cost, mechanical and electrical stability, low-temperature processability and large-area processability. They are widely used in applications pertaining to flexible displays, wearable devices, radio frequency identification (RFID) tags, e-skin, biosensors, and flexible integrated circuits. However, organic thin film transistors are still inferior to silicon-based technologies, trailing behind in several critical performance metrics such as low mobilities and high operational voltages. These challenges can be mitigated using metal oxides, which, owing to their high work function and stability, can enhance the parameters of OTFT devices. This review aims to provide insights into the usage of metal oxides in organic thin film transistors and highlight their contribution as hole injection layers (HILs), charge transport complexes (CTCs), bilayer source–drain (S–D) electrodes and gate dielectrics.

Received 14th March 2025,
Accepted 29th August 2025

DOI: 10.1039/d5ma00231a

rsc.li/materials-advances



## 1. Introduction

Organic thin film transistors (OTFTs) have emerged as an important economical transistor technology in various applications due to their unique properties. Organic thin film transistors are a type of field effect transistors containing an organic semiconductor layer. Organic thin film transistors provide advantages over inorganic silicon-based semiconductors for their flexibility,[1] light weight,[2] biocompatibility,[3] solution processability,[4] printed fabrication,[5] large-area processability,[6] and cost effectiveness[7]. They are used in various applications such as flexible displays,[8] wearable devices,[3,9] radio frequency identification (RFID) tags,[10] e-skin,[2,11] biosensors,[12] and flexible integrated circuits.[13,14] Despite the remarkable progress in organic thin-film transistor (OTFT) technology, achieving high-performance and stable devices remains a significant challenge. Compared to silicon-based thin-film transistors, OTFTs continue to be inferior, encountering limitations such as inconsistent physical models, lower charge carrier mobilities, higher contact resistance, and reduced environmental stability, hampering their widespread implementation in practical applications. Thus, to address these issues, doping has emerged as a key strategy for enhancing the electronic properties of OTFTs. By introducing charge carriers *via* p-dopants and n-dopants, significant improvements in the performance and stability of organic semiconductors can be achieved. Metal oxide interlayers improve device parameters by easing hole injection, tuning contact engineering, and even by their excellent dielectric properties.

Among the p-dopants, one of the most widely used molecular dopants is 2,3,5,6-tetrafluoro-7,7,8,8-tetracyanoquinodimethane ($F_4$-TCNQ),[15] a strong electron acceptor with a low-lying LUMO (electron affinity) of 5.2 eV capable of oxidising the HOMO of most organic semiconductors. Molecular doping with the $F_4$-TCNQ molecule is desirable due to its efficient blending with various organic host materials and ordered arrangement, leading to improved charge transport characteristics such as enhanced mobilities, high on/off current ratios, reduced threshold voltage and decrease in contact resistance.[16] Beyond molecular dopants, elemental species such as diatomic halogens ($I_2$, $Br_2$, and $Cl_2$) have been investigated as p-dopants[17]. These species facilitate the formation of charge transfer complexes (CTCs), which enhance the hole transport in organic semiconductors.[18] Another category of p-dopants includes Brønsted and Lewis acids, such as tris(pentafluorophenyl)-borane (BCF),[19] iron chloride ($FeCl_3$),[20] tris(4-bromophenyl)-ammoniumyl hexachloroantimonate (magic blue),[21] antimony pentachloride ($SbCl_5$)[22] and molybdenum tris(dithiolene) complexes ($Mo(dt)_3$),[23] to obtain higher device performances such as higher mobilities, thermoelectric efficiency and optoelectronic applications. n-Dopants have been utilised in organic electronics including elemental dopants such as lithium (Li), sodium (Na), potassium (K), and caesium (Cs)[24] and inorganic alkali salts such as lithium carbonate ($Li_2CO_3$),[25] sodium carbonate ($Na_2CO_3$),[26] and caesium carbonate ($Cs_2CO_3$),[27] which are applied to obtain a reduction in the electron injection barrier.

*Department of Chemistry, Manipal Institute of Technology, Manipal Academy of Higher Education, Manipal 576 104, Karnataka, India.*
*E-mail: poornima.nayak@manipal.edu*

Organic semiconductor devices extensively employ metal oxides as p-dopants due to their high work function, high electron affinity, high sensitivity, and transparency. Interlayers of metal oxides also reduce the issue of high contact resistance at the interface between the organic semiconductor and the electrode. The differences in work function between the electrode and highest occupied molecular orbitals (HOMO) can result in barriers and increase the contact resistance. The high work function of metal oxides enhances the energy level alignment between the metal electrode and organic semiconductor, allowing Schottky to Ohmic conversion. Metal oxides can serve as electron acceptors, undergoing electron transfer with the HOMO of organic materials, generating holes in the organic material, and effectively p-doping. Thus, metal oxides provide an efficient method to decrease the barriers and contact resistance to obtain high-performance OTFTs.

This review focuses on the different metal oxides employed in enhancing the efficiency of OTFTs and their role as dopants in OTFTs. Finally, it is concluded with the limitations and scope of this research area.

## 2. Transition metal oxides as dopants in OTFTs

Transition metal oxides (TMOs) have been gaining widespread interest in organic thin film transistors (OTFTs) due to their high work function, stability and role as an interfacial layer. They are ideal for forming ohmic contacts at the metal oxide/organic semiconductor interface. They play an essential role as hole injection layers (HILs), charge transport complexes (CTCs), source–drain (S–D) electrodes and gate dielectrics. The commonly used metal oxides include $MoO_3$, $V_2O_5$, $WO_3$, ZnO, CuO, and $ReO_3$, which can help realise applications for the next generation of organic electronics.

Among them, molybdenum oxide ($MoO_3$)[28] is an p-type dopant commonly used in organic thin film transistors. $MoO_3$ facilitates efficient charge transfer at the metal oxide/organic semiconductor interface owing to its high work function. Thus, it is used as hole injection layers, enhancing organic thin film transistors by increasing their charge injection, stability, and conductivity and reducing their contact resistance.[6,29] $MoO_3$ helps in energy level alignment (ELA) due to its high work function and reducing the energy level mismatch with organic semiconductors. Additionally, it form charge transport complexes (CTCs), enhancing the generation of free carriers and carrier mobilities. It is also employed in source–drain (S–D) electrodes due to its electrical properties as an inexpensive alternative to Au and Ag electrodes.[30–32]

Similarly, vanadium oxide ($V_2O_5$)[33] and tungsten oxide ($WO_3$)[34] are also employed extensively in organic thin film transistors as p-type dopants in source–drain (S–D) electrodes and hole injection layers. $V_2O_5$ and $WO_3$ are used to reduce contact resistance, enhance the charge carriers, increase the field effect mobility and match with the highest occupied molecular orbital (HOMO) of organic semiconductors, thereby providing energy level alignment (ELA).[35,36]

Owing to the versatile nature of zinc oxide (ZnO), it has been employed as a dopant in organic thin film transistors due to its wide band gap, transparency, and high field-effect mobility. ZnO nanoparticles are used in organic devices as n-type dopants, generating electrons and enhancing the free charge carriers and electron acceptors in p-type organic semiconductors, enhancing hole transport. They improve the device performance due to their capability to produce a low sub-threshold voltage, low amount of hysteresis, enhanced current ratio ($I_{ON}/I_{OFF}$), and reduced trap density, thereby forming good ohmic contact. ZnO nanoparticles have also been used in hybrid multilayer organic–metal oxide heterojunctions, showing high field effect mobility and high operational stability.[37,38]

Another transition metal oxide that has been extensively used is copper oxide (CuO),[39] which owing to its high work function serves as a means to reduce the threshold voltage, resulting in low operational voltages and hole injection layers to enhance the conductivity in organic thin film transistors. CuO films in organic thin film transistors have been investigated owing to their ability to shift the threshold voltages to lower values by controlling the trap densities in the OTFT channel layers.[40] Similarly, CuO is employed as a source–drain (S–D) bilayer electrode in organic thin film transistors, enhancing the device performance.[41]

Rhenium oxides have been explored to provide an alternative method to overcome the compatibility issues observed during co-evaporation at the high evaporation temperatures for metal oxides. Rhenium oxides are known to have a low evaporation temperature, improving the compatibility in low melting point organic semiconductors. $ReO_3$ has a melting point of 340 °C and $Re_2O_7$ has a melting point of 225 °C, thus improving the compatibility with organic semiconductors. Rhenium oxides showed a considerable improvement in the mobilities of organic devices and utilized as hole injection layers (HILs).[42–44]

High dielectric constant ($\kappa$) metal oxides such as zirconium oxide ($ZrO_2$),[45] hafnium oxide ($HfO_2$),[46] and aluminium oxide ($Al_2O_3$)[47] and rare earth metal oxides such as neodymium oxide ($Nd_2O_3$)[48] and lanthanum oxide ($La_2O_3$)[49] are used in the gate dielectric in organic thin film transistors. The use of high $\kappa$ metal oxides results in organic thin film transistors with low operational voltages, high operational stability, low leakage current density, and high capacitance.[50–52]

## 3. Function of metal oxides in OTFTs

### 3.1 Metal oxides as hole injection layers (HILs)

Transition metal oxides (TMOs), such as CuO, $WO_3$, $MoO_3$, $ReO_3$, $Ni_2O_3$, $Co_3O_4$ and $V_2O_5$, owing to their high work function, reduced contact resistance, wide band gap, high stability, ease of processing and low cost, have been gaining significant attention as hole injection layers (HILs) (Fig. 1). Transition metal oxide interlayers are employed in organic thin film transistors, serving as an ohmic contact and increasing hole injection, thus enhancing the device performance. By inserting

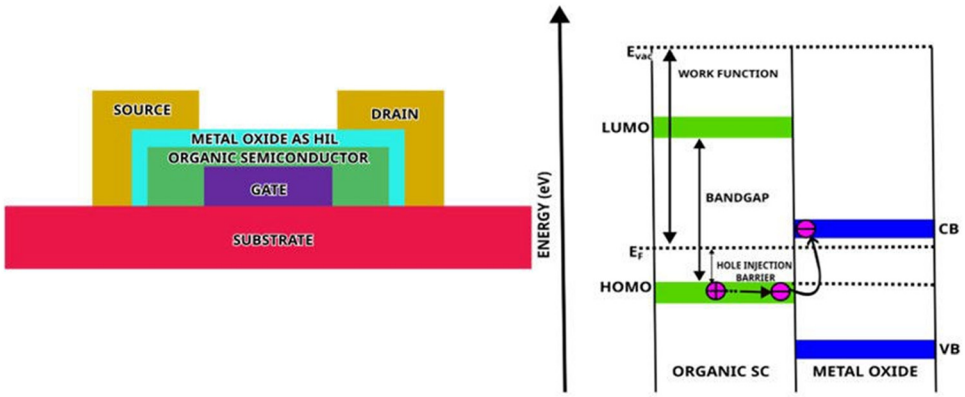


Fig. 1 Schematic representation of hole injection layer in an OTFT and schematic of the hole injection mechanism between the conduction band of metal oxide and highest occupied molecular orbital (HOMO) of an organic semiconductor.

an injection layer electrode between a metal and an organic semiconductor, a reduced hole injection barrier and suppressed contact resistance are achieved.[53–55]

Fig. 1 illustrates how holes are injected from the valence band or conduction band of a metal oxide into the highest occupied molecular orbital (HOMO) of an organic semiconductor due to the charge transfer that occurs by electron extraction from the HOMO of the organic semiconductor to the valence band or conduction band of a metal oxide. Metal oxides such as $MoO_3$, $V_2O_5$ and $WO_3$, which are known for their high work functions, are efficient at creating minimal energy barriers when used as an interface layer with organic semiconductors that have deeply positioned HOMO levels. The utilization of metal oxides is crucial in optimizing the device properties in organic thin film transistors. By reducing the injection barrier height at the interface, they enhance the amount of charge that can be introduced into the channel. Consequently, a reduction in the injection barrier promotes lower power consumption. These metal oxides also exhibit the ability to suppress short channel effects, offering scalability and stability for the development of low-voltage and short-channel organic devices. Energy level alignment by metal oxides minimizes the energy mismatch, and thus helps in efficient hole injection, allowing efficient operation and improving the working of organic devices.[56,57]

The presence of a large charge injection barrier in an OTFT is due to the mismatch in the work function or formation of interfacial states, which is seen to critically hamper the device performance. The consequent non-linear relation between the current and applied voltage and reduction in effective gate electric field weakens the ability of the gate to induce an accumulation layer and reduces the field effect mobility compared to the intrinsic mobility. Yun *et al.*[58] investigated the use of molybdenum oxides ($MoO_x$) as a hole injection layer in a DBTTT semiconductor OTFT, functioning to reduce the contact resistance and increase the conductivity. A typical metal/organic semiconductor is prone to non-linear *I–V* characteristics at low voltages, which is attributed to its large charge injection barriers. The deposition of $MoO_x$ as a hole injection layer resulted in a linear relationship in the *I–V* characteristics of a device, indicating a transition from Schottky to Ohmic contact. The presence of $MoO_x$ removes the inconsistency that persists between intrinsic mobility and field effect mobility in the linear regime. A field effect mobility of 3.68 $cm^2\ V^{-1}\ s^{-1}$ was obtained using a bare Au electrode, whereas when an $MoO_x$ film layer was incorporated in the Au electrode, the obtained field effect mobility in the linear regime was 6.47 $cm^2\ V^{-1}\ s^{-1}$ for the $MoO_x$ (5 nm)/Au layer and 6.72 $cm^2\ V^{-1}\ s^{-1}$ for the $MoO_x$(10 nm)/Au layer. These values are consistent with the estimated intrinsic mobility, indicating a significant decrease in contact resistance, and thus increase in the field effect mobility. The use of an Al electrode as a cheaper alternative to Au was also explored, which required 75 nm-thick $MoO_x$ films. A similar enhanced performance was obtained for an $MoO_x$/Al layer with a field effect mobility of 5.77 $cm^2\ V^{-1}\ s^{-1}$ in the linear regime. Liu *et al.*[59] found that the interfacial contact resistance is diffusion limited. Experimental analysis of the charge injection in the metal/organic semiconductor showed that non-Ohmic contacts have a characteristic hook-shaped conductance/drain voltage relationship. To overcome this effect, Liu *et al.* utilised metal oxides, $MoO_3$ and $V_2O_5$, as charge injection layers, as well as other strategies such as bulk doping, interlayer and high $\kappa$ dielectric. The metal oxide charge injection layer increased the mobilities and reduced the contact resistance. At gate voltage $V_g = -80$ V, the bare metal/organic semiconductor of Mo/P3HT obtained mobilities of $4.5 \times 10^{-3}$ $cm^2\ V^{-1}\ s^{-1}$, while the OTFTs with $MoO_3$ and $V_2O_5$ obtained mobilities of $2.1 \times 10^{-2}$ $cm^2\ V^{-1}\ s^{-1}$ and $1.9 \times 10^{-2}$ $cm^2\ V^{-1}\ s^{-1}$, respectively. The recombination rates also are enhanced due to the decrease in injection barrier from the metal oxide injection layer. These results show that contact resistance engineering goes hand in hand with enhancing the mobility in OTFTs and the decrease in interfacial contact resistance as the carrier mobility increases confirms that both the charge injection and interfacial contact resistance are diffusion limited.

The use of high work function metal oxides does not guarantee the ability to form an Ohmic contact. There are various

factors that determine the formation of an ohmic contact, especially the energy level alignment. For a highly efficient ohmic contact, the bulk-limited current should be close to the injection limited current. Yoo *et al.*[60] demonstrated the formation of ohmic contacts by the deposition of thin film metal oxides such as $MoO_3$ and $ReO_3$ between metal/organic semiconductor interfaces, obtaining a near perfect ohmic contact with the use of $ReO_3$ injection layer. $MoO_3$ and $ReO_3$ were used due to their high electron affinity and hole injection properties. The current density vs electric field curve, *i.e. J–F* characteristics of the hole-only devices, were measured with and without a metal oxide interlayer. The *J–F* curve of the hole-only devices without a metal oxide interlayer showed non-linear characteristics, whereas the hole only devices with a metal oxide interlayer showed comparable linear characteristics, showing that the insertion of an interlayer enhanced the current densities. The $ReO_3$ interlayer obtained a near perfect hole injection efficiency of close to 100% and gave a significant increase in current density compared to the $MoO_3$ interlayer, with one magnitude larger than $MoO_3$ interlayer. Ultraviolet photoelectron spectroscopy (UPS) was the method employed to measure the hole injection barriers, which disclosed that the hole injection barriers obtained for $MoO_3$/organic semiconductor was 0.41 eV and that for $ReO_3$/organic semiconductor was 0.38 eV, showing a considerable reduction in barriers compared to the substrate/organic semiconductor devices without metal oxides (1.64 eV). The enhanced device properties is due to the p-type doping caused by the formation of a charge transfer complex, which can be confirmed by the increase in the $Mo^{v}$ and $Re^{iv}$ peaks as a result of the reduction of the metal oxide films by NBP.

The interface structure of the device, whether metal oxide is deposited on an organic semiconductor (inverted deposition) or an organic semiconductor is deposited on metal oxide (non-inverted deposition) plays an important role in the device performance. When an organic semiconductor is deposited onto a transition metal oxide structure, its characteristics closely resemble those of only the organic semiconductor film and a larger part of the organic semiconductor remains undoped. This is attributed to the high density and stability of the underlying metal oxide layer, preventing any diffusion. In contrast, a structure that employs a transition metal oxide on an organic semiconductor layer results in the diffusion of the metal oxide onto the organic semiconductor and is shown to depend on the thermal stability of the organic semiconductor. Beck *et al.*[61] studied inverted deposition and non-inverted deposition at organic (CBP)/metal oxide ($MoO_3$) interfaces using IR spectroscopy. The intensities of the CBP cations were higher in the inverted structure of $MoO_3$ deposited on CBP compared to the non-inverted deposition of CBP on $MoO_3$. This was principally due to the difference in mechanism, where in the inverted structure, the diffusion of metal oxide is extended to up to 10 nm, while in the non-inverted structure, the space charge region is found to be up to 2 nm, and thus only limited CBP molecules are affected. Zhao *et al.*[62] systematically investigated the impact of deposition order on the optical and electronic properties of $MoO_3$ and NPB interfaces. The absorption spectrum of the non-inverted deposition of NBP (10 nm) on $MoO_3$ (3 nm) closely resembled that of the pure NBP layer. Alternatively, the absorption spectrum of the inverted deposition of $MoO_3$ (3 nm) on NBP (10 nm) exhibited two additional absorption peaks compared to pure NBP films, proving the diffusion of $MoO_3$ into NBP. These spectral features resembled those of $MoO_3$-doped NBP films, suggesting the effective intermixing of $MoO_3$ on the NBP layer. The diffusion of $MoO_3$ studied with NBP, TCTA and CBP showed an increase in diffusion as a function of their evaporation temperature. Given that the evaporation temperatures of metal oxides is much higher than those of organic semiconductors, the inverted interface always results in the diffusion of metal oxide in organic semiconductors. White *et al.*[63] further reported that diffusion does not occur into metal oxides in the non-inverted deposition order due to the higher stability, higher density and significant difference in evaporation temperatures between the organic materials and $MoO_3$. In contrast, in the inverted structure, the deposited metal oxides have higher kinetic energy to be able to diffuse into the organic layer. The diffusion of metal oxide into the organic semiconductor results in electron transfer, resulting in the p-doping of organic semiconductors. This leads to band bending, which can be characterised by the shifts in the C1s peak to a lower binding energy after CBP donates charge to $MoO_3$, while the Mo3d peak shifts to a higher binding energy after receiving the charge. The formation of new core–shell peaks, $C^{x+}$ and $Mo^{x+}$, provided evidence for charge transfer, and consequently it was observed that ratio of $C^{x+}$ to C–C bond state showed a decrease for molecules with a higher molecular mass compared to molecules with a lower molecular mass. Diffusion was shown to be a function of molecular mass, as observed in the comparison of mCP, CBP, and mCBP, which exhibited the most diffusion, with molecules of larger molecular mass, such as NPB, TCTA, and MTDATA, exhibiting the least diffusion. This result is consistent with the high kinetic energy model, given that the thermal stability of organic molecules with weak intermolecular forces is largely dictated by their molecular mass. Although the diffusion of transition metal oxides onto organic semiconductors can be utilised to obtain enhanced hole injection and is a simpler alternative to the complex process of controlled doping of metal oxides in organic semiconductors, it has been associated with device instability and poor reproducibility. The diffusion of metal oxides into organic semiconductors is often unpredictable and results in variable device parameters such as change in threshold voltage and on/off current ratio. Recent advances involve a multilayer interface that employs a blocking layer between the organic semiconductor and metal oxide to prevent diffusion, and thus improve the device stability. Yang *et al.*[64] utilised a metal/metal oxide/organic multilayered interface contact (MIC) source–drain electrode, which achieved higher device stability. They proposed an organic multilayer interface containing an organic buffer layer (OBL) such as such as 1,3-bis(carbazol-9-yl)benzene (mCP), 4,4′-bis(carbazol-9-yl)-biphenyl (CBP), 4,4′-bis(carbazole-9-yl)-2,2′-dimethylbiphenyl (CDBP),

*N*,*N*′-bis(naphthalen-1-yl)-*N*,*N*′-bis(phenyl)-benzidine (NPB), 1,4-bis(triphenylsilyl)benzene (UGH-2), di-[4-(*N*,*N*-di-*p*-tolyl-amino)-phenyl]cyclohexane (TAPC), and 4,4′,4″-tris(carbazol-9-yl)triphenylamine (TCTA) among the organic semiconductor, copper phthalocyanine and metal oxide $MoO_3$ to prevent the diffusion of the metal oxide. The devices with OBL obtained a higher on/off current given that the off current in these devices did not intensely increase, as was shown in the devices without OBL due to the diffusion of metal oxides in the organic semiconductors. Hence, the operation stability also increased considerably. The on/off current ratio of the devices without OBL was $1.10 \times 10^2$, while that of the devices with organic buffer layers such as mCP was $1.33 \times 10^3$, CBP was $1.90 \times 10^3$, CDBP was $2.67 \times 10^3$, NBP was $3.72 \times 10^3$, UGH-2 was $2.89 \times 10^3$, TAPC was $1.07 \times 10^2$ and TCTA was $4.94 \times 10^2$. The obtained contact resistance in the devices with the $MoO_3$/organic semiconductor and device with OBL NBP was 0.51 MΩ and 0.76 MΩ, respectively, showing that $MoO_3$ can still efficiently reduce the contact resistance, even in the presence of OBL. However, due to the lack of literature on the use of OBL, the selection of an appropriate OBL for OTFT devices is limited.

Kim *et al.*[65] used $VO_2$ as a hole injection layer (HIL) and studied the electrical properties by using photoemission spectroscopy. The measured UPS spectra of the normalized secondary electron cutoff (SEC) and background removed the HOMO region during NPB deposition on the $VO_2$/FTO substrate, which was similar to previous reports, showing a shallow valence band maximum (VBM) close to Fermi level ($E_F$). The valence band maximum (VBM) is measured to be 0.45 eV below the Fermi level ($E_F$), corresponding to the hole injection barrier ($\phi_h$) from fluorine-doped tin oxide (FTO) to $VO_2$. According to the obtained UPS spectrum, it is evident that there is an increase in work function ($\psi$) from 4.02 eV for only FTO to 5.66 eV for $VO_2$/FTO, aligning with the highest occupied molecular orbital (HOMO) of NBP, and consequently reducing the hole injection barrier. Thus, $VO_2$ acts as a hole injection layer (HIL), reducing the original hole injection barrier ($\phi_h$) with a step-like energy level alignment called the ladder effect, wherein the large barrier is divided into two smaller barriers, *i.e.* the first hole injection barrier ($\phi_h$) from FTO to $VO_2$ is 0.45 eV and the second $\phi_h$ from $VO_2$ to NPB is 0.14 eV. XPS measurements further helped confirm the $VO_2$ phase to be consistent with the valence band shape obtained in the UPS measurements. The areal ratio was determined to be 1.0 : 1.9 between the V 2p and O 1s and is consistent with the stoichiometric $VO_2$ phase expected. The V $2p_{3/2}$ peak observed at 516.2 eV is characteristic of $V^{4+}$, similar to the reported values such as $V^{5+}$ ($V_2O_5$) at 517.2 eV and $V^{3+}$ ($V_2O_3$) at 515.3 eV for vanadium. The hole injection layer of $VO_2$ provides p-doping due to the electron transfer from the NBP HOMO and conduction band as well as the valence band of $VO_2$, leaving behind mobile holes. This double hole injection of device shows the versatile nature of $VO_2$ and can considerably enhance the device metrics, showing enhanced *J*–*V* characteristics for $VO_2$/FTO compared to the devices without hole injection, providing potential for transparent anodes.

Another key consideration is the ability to fine tune the work function of metal oxides to obtain the best possible performance in OTFTs. Metal oxides are prone to air oxidation, resulting in a decrease in work function.[56] Thus, different work function values are obtained based on the conditions, requiring the work function to be tuned for specific values. Yao *et al.*[66] was able to modify the work function of $MoO_3$ by employing different deposition techniques, during which either the ratio of $O_2$ to the total sum of $O_2$ and Ar was varied or the time of oxygen plasma treatment was varied. The work function increased from 4.85 eV to 5.80 eV, wherein a linear increment was observed in the ratio of $O_2$ to the total sum of $O_2$ and Ar of 0.1 to 0.2, after which there were only small changes in work function in the range of 0.2 to 0.3 $O_2$ to the total sum of $O_2$ and Ar. Alternatively, the work function based on oxygen plasma treatment after Mo deposition increased from 4.66 eV to 5.30 eV for a treatment time in the range of 0 to 30 seconds. Similar to varying the ratio of $O_2$ to the total sum of $O_2$ and Ar, the work function reached saturation after an oxygen plasma treatment time of 35 to 45 seconds. The surface smoothness obtained by atomic force microscopy revealed that as the ratio of $O_2$ to the total sum of $O_2$ and Ar increased from 0.1 to 0.3, the RMS roughness decreased from 0.71 nm to 0.33 nm. A similar decrease in RMS roughness from 0.83 nm to 0.51 nm was observed upon varying the oxygen plasma treatment time from 0 to 45 seconds. The XPS data shows that on increasing the ratio of $O_2$ to the total sum of $O_2$ and Ar, the peak of the $Mo^{4+}$ state decreases, while there is an increase in the $Mo^{6+}$ and $Mo^{5+}$ peaks. As the gas ratio increased from 0.1 to 0.2, the $Mo^{5+}$ peak area decreased from 61.2% to 1%, while simultaneously the $Mo^{6+}$ peak increased from 70% to 84.7%. This was attributed to the increase in oxygen anion during deposition by increasing the gas ratio, thus increasing the work function. The XPS data for oxygen plasma treatment shows a similar shift in peaks towards higher binding energies as the treatment time increases. As the treatment time increased from 5 to 45 seconds, the peak area of $Mo^{5+}$ decreased from 23.5% to 13.8%, while peak area of $Mo^{6+}$ increased from 70.0% to 84.7%. The OTFT device parameters such as on/off current ratio, subthreshold slope and the threshold voltage obtained with and without oxygen plasma treatment were $1 \times 10^6$ and $1 \times 10^4$, 1 and 1.4, and −3.8 V and −14.5 V, respectively, showing that the device could be optimized by modifying its work function.

Metal oxides can also be explored as the hole injection layer in organic phototransistors. The properties of metal oxides such as wide bandgap, optical properties and transparency with optical transmittance greater than 70% in the visible region enable the preparation of low cost and efficient organic phototransistor devices. Park *et al.*[67] reported that transition metal oxide-based (TMOs) buffer layers significantly enhanced the device parameters in organic phototransistors. A transparent indium zinc oxide (IZO) electrode with molybdenum oxide ($MoO_3$) buffer layer was used as the hole injection layer to improve the electrical conductivity as well as due to its optical transparency in the visible region. The presence of metal oxide was shown to reduce the hole injection barrier, which

was confirmed by measuring the hole injection barrier values using ultraviolet photoelectron spectroscopy (UPS). The measured values of the hole injection barrier between IZO and the pentacene layer without the presence of buffer $MoO_3$ was found to be 0.65 eV, whereas the hole injection barrier between IZO/$MoO_3$ and the pentacene layer was found to be 0.42 eV, with a decrease of 35% in the presence of a metal oxide buffer layer. The device showed excellent electrical properties with a mobility of 1.40 $cm^2\ V^{-1}\ s^{-1}$, threshold voltage of −13.8 V, subthreshold slope of −4.54 V $decade^{-1}$, on/off current ratio of $10^5$, and optical properties with high transparency of 70.4% average transmittance in the visible region and photoresponsivity of 54.8 A $W^{-1}$. The device prepared on a cellulose nanofibrillated fibre substrate was also confirmed to be biodegradable, providing an environmentally friendly electronic device. Jung *et al.*[68] investigated the use of $MoO_3$-doped pentacene to enhance the electrical performance of UV photodetectors. A 10 nm $MoO_3$ layer enhanced the OTFT device metrics with a hole mobility of $1.71 \times 10^{-1}$ $cm^2\ V^{-1}\ s^{-1}$, threshold voltage of −16.69 V and on/off current ratio of $2.5 \times 10^3$ compared to the pristine pentacene OFET devices, exhibiting the hole mobility $5.16 \times 10^{-3}$ $cm^2\ V^{-1}\ s^{-1}$, threshold voltage of −54.26 V and on/off current ratio of $1.7 \times 10^{-4}$. Again, this was attributed to the considerable reduction in contact resistance, which was approximately half of that of the pristine pentacene OFET devices. The $MoO_3$-doped OFETS also showed increased photosensitivity, with an increase in photoresponsivity from $3.2 \times 10^2$ to $1.0 \times 10^4$ A $W^{-1}$ upon the introduction of $MoO_3$. Although the device performance was considerably shown to increase, the use of OFET devices as photodetectors has been restricted due to their high power consumption. High power dissipation of $1.0 \times 10^{-4}$ W $cm^{-2}$ was calculated for $MoO_3$-doped OFETs, leading to the lower energy efficiency of the photodetectors. In comparison, an $MoO_3$-doped suboptimal source gated transistor (sSGT) device showed a significantly lower $P_{diss}$ of $3.04 \times 10^{-7}$ W $cm^{-2}$, providing an enhanced optical power efficiency in photodetectors. Thus, further improvements in power efficiency need to be realised for the application of OFETs in photodetectors.

### 3.2 Metal oxides as charge transfer complexes (CTCs)

Transition metal oxides (TMOs) having high electron affinity can interact with wide band gap organic semiconductors to form a charge transfer complex. As shown in Fig. 2, these complexes arise from the interaction between the electron-rich organic semiconductors and the electron-deficient transition metal oxides (TMOs), leading to partial electron transfer. Transition metal oxides (TMOs) play a role in organic thin-film transistors (OTFTs) by forming charge transfer complexes (CTCs) with organic semiconductors, and the corresponding interaction provides significant enhancement of the electronic properties of the devices such as lowering the injection barrier for holes, increasing the current density and conductivity and improving the charge injection efficiency and mobility in organic semiconductor devices. This mechanism of charge transport complex is capitalized by bulk doping of metal oxides, as well as interlayers such as hole injection layers, and even

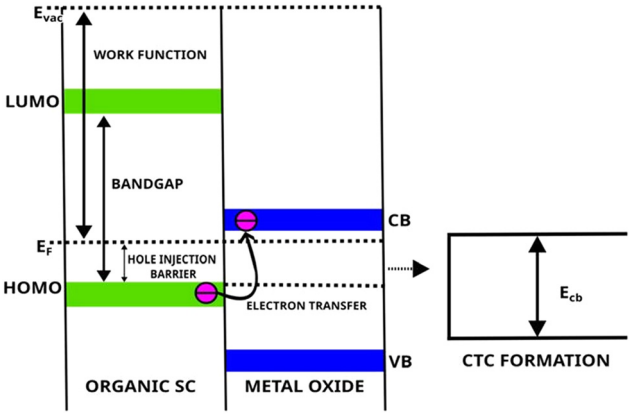


Fig. 2 Schematic representation of the charge transport complex between a metal oxide and an organic semiconductor.

source/drain bilayer electrodes to obtain high-performance OTFTs. Yan *et al.*[69] utilized $MoO_3$ as a buffer layer, enhancing the OTFT device parameters by capitalizing on charge transfer complex formation. OTFT devices were constructed using pentacene as the organic semiconductor and 4,4″-tris(3-methylphenylphenylamino)triphenylamine (m-MTDATA) and molybdenum oxide ($MoO_3$) as buffer layers. According to the output curves in the saturation regime ($V_{ds}$ = −100 V), the pentacene:m-MTDATA:$MoO_3$ device demonstrated an outstanding effective mobility ($\mu_{eff}$) of 0.72 $cm^2\ V^{-1}\ s^{-1}$ and a reduced threshold voltage ($V_{th}$) of −13.4 V, while devices consisting pentacene:$MoO_3$ obtained $\mu_{eff}$ of 0.36 $cm^2\ V^{-1}\ s^{-1}$ and $V_{th}$ of −33.7 V. The m-MTDATA:$MoO_3$ device obtained $\mu_{eff}$ of 0.40 $cm^2\ V^{-1}\ s^{-1}$ and $V_{th}$ of −20.7 V. At a fixed gate voltage of −100 V, the obtained $I_{ds}$ *vs.* $V_{ds}$ curves indicated that the pentacene:m-MTDATA:$MoO_3$ device exhibited the best drain current of 38.05 μA compared to the drain current values in pentacene:$MoO_3$ of 12.93 μA and m-MTDATA:$MoO_3$ of 23.91 μA. This significant enhancement in drain current is primarily due to the formation of charge transfer complexes (CTCs) in the buffer layer. These CTCs are critical, given that they greatly increase the hole density and improve the alignment of energy levels. AFM measurements convey that the application of metal oxide resulted in smoother films with a considerable reduction in RMS roughness from 4.33 nm for the pure pentacene film to 3.21 nm in pentacene:m-MTDATA:$MoO_3$. Thus, the OTFT devices exhibited a significant improvement in device parameters such as high effective mobility, reduced threshold voltage, increased hole injection to organic semiconductors and lower total resistance.

As mentioned before, metal oxides serve as an effective tool to enhance the performance of organic phototransistors owing to their wide band gap and transparency. The formation of charge transfer complexes between a heterojunction of an organic semiconductor and metal oxide can be an effective solution to enhance the performance of organic phototransistors for fiber communication, especially in the second near infrared region. Wang *et al.*[70] used the CTC principle to enhance the device properties of on organic phototransistor,

obtaining near infrared detection greater than 1000 nm. A heterojunction CTC was prepared using 4,4″-tris(3-methylphenylphenylamino)triphenylamine (m-MTDATA) as an electron donor and tungsten oxide ($WO_3$) as an electron acceptor in a pentacene organic phototransistor. The CTC mechanism is explained by intermolecular charge transfer transitions from the highest molecular orbital of m-MTDATA (−5.1 eV) into the corresponding conduction band of $WO_3$ (−4.6 eV). Thus, an electron from the HOMO of m-MTDATA can transfer into the conduction band of $WO_3$, while holes can be injected from $WO_3$ to the HOMO of m-MTDATA, causing band bending. The device properties were investigated by studying the output characteristics of organic phototransistors with varying CTC layer thicknesses. The devices exhibited enhanced mobilities as the thickness of the CTC layer increased from 20 nm to 30 nm, functioning as an enhancing layer up to a thickness of 30 nm, after which it decreases, functioning as a depletion layer. The devices with an organic phototransistor comprised of a 20, 30, 40, 50 and 60 nm CTC layer provided the mobility of $2.79 \times 10^{-2}$, $4.39 \times 10^{-2}$, $4.18 \times 10^{-2}$, $2.45 \times 10^{-2}$, and $1.60 \times 10^{-2}$ $cm^2\ V^{-1}\ s^{-1}$, respectively. On increasing the thickness of CTC, the absorption of near-infrared light increased, as well as the defect states; however, an increase in thickness can cause a decrease in the charge transport quality. Hence, the highest photoresponsivity of 36.76 mA $W^{-1}$ was obtained with the CTC thickness of 40 nm and highest mobility and dark current at the thickness of 30 nm by balancing the respective trade-offs. Yin *et al.*[71] utilised CTC formation between $V_2O_5$ and 2T-NATA to obtain copper phthalocyanine (CuPc) organic phototransistors, which allows photodetection in the near infrared-II region of 1000–1700nm. Intermolecular charge transfer from the HOMO of 2T-NATA at −5.0 eV and conduction band of $V_2O_5$ at −4.8 eV resulted in a photosensitive film. Consequently, electron extraction from the HOMO of 2T-NATA to the conduction band of $V_2O_5$ enables the formation of CTC, which greatly enhances the metrics of organic phototransistor devices by p-doping, enabling absorption in NIR-II. Similar charge transfer can also occur between $V_2O_5$ and $F_{16}$CuPc, resulting in electron transfer from the LUMO to conduction band and charge transfer between $V_2O_5$ and CuPc, resulting in electron transfer from the HOMO to $V_2O_5$ through carrier tunnelling and heterojunction accumulation with holes in CuPc and electrons in F16CuPc. The devices prepared with different fabrication methods utilising these mechanisms exhibit p-type, n-type and ambipolar characteristics, allowing the optimization of CTC organic phototransistors. It was seen that the $V_2O_5$ and 2T-NATA CTC resulted in inhibition of electron transport, causing weak n-type characteristics. Thus, to realise ambipolar nature, the n-type characteristics were enhanced by incorporating F16CuPc as well as optimizing the ratio of CTC. A device with ambipolar nature was attained by CTC of $V_2O_5$ : 2TNATA (1 : 2), showing field effect mobilities of $7.18 \times 10^{-5}$ $cm^2\ V^{-1}\ s^{-1}$ and $6.60 \times 10^{-5}$ $cm^2\ V^{-1}\ s^{-1}$, as well as the maximum photoresponsivity of 0.115 A $W^{-1}$ and 2.600 A $W^{-1}$ in n-type and in p-type, respectively.

At the interface between an organic semiconductor, acting as an electron donor, and p-type metal oxide, acting as an electron acceptor, the corresponding charge transport complex formed greatly helps reduce the activation energy for the conduction of charge carriers, improving the device performance. Lee *et al.*[72] demonstrated that employing electron acceptor metal oxides such as $MoO_3$ to form charge transfer complexes (CTCs) with organic hole semiconductors enhances the charge transport, and thus the overall mobility of organic semiconductors. Bulk doped NBP and the $MoO_3$/NBP heterostructure exhibited additional absorption peaks at the wavelength of 500 nm, indicating that a CTC is formed between $MoO_3$ and NBP. The heterojunction of $MoO_3$/NBP provided enhanced conductivity, which was attributed to the increased charge carrier density due to the formation of CTC. The Beer–Lambert law analysis at 350 nm shows an initial high absorption coefficient value due to the vertical orientation of the NBP molecules. As the thickness increases, the increase in randomly aligned molecules can explain the constant absorption coefficient. Alternatively, at the 500 nm absorption band, a constant absorption coefficient is observed, indicating the independent nature of the molecular orientation with thickness. By utilising the principle of the CTC in a metal oxide/organic semiconductor interface, a significant reduction in the activation energy ($E_a$) of $MoO_3$ from 0.23 eV to 0.18 eV was achieved. This decrease in $E_a$ was attributed to the formation of charge transfer complexes, which generate additional charge carriers, consequently filling the deep trap states associated with the electronic and structural defects in $MoO_3$ and increasing the mobilities. Lim *et al.*[73] studied the formation of charge transfer complexes (CTC) and the generation of free carriers in the heterojunctions of several organic semiconductors and transition metal oxides (TMOs) using UV-visible-near IR (UV-VIS-NIR) spectroscopy and the transmission line method (TLM). The formation of a charge transfer complex was confirmed by studying the absorption spectrum of the organic semiconductor and transition metal oxide bilayer, which shows intrinsic absorption peaks of its individual materials ($MoO_3$, 2TNATA, NPB, TCTA, and CBP) at specific wavelengths and additional peaks in the short wavelength region (400–600 nm) and long wavelength region (1000–2000 nm), proving the charge transfer from the organic semiconductor to transition metal oxide. The short wavelength peak obtained for $MoO_3$/2TNATA was located at 474 nm, $MoO_3$/NPB at 496 nm, $MoO_3$/TCTA at 420 nm and $MoO_3$/CBP at 441 nm and the long wavelength peak obtained for $MoO_3$/2TNATA at 1329 nm, $MoO_3$/NPB: at 1483 nm, and $MoO_3$/TCTA at 1560 nm and $MoO_3$/CBP had no distinct peak. The CTC peaks are obtained because of the charge transfer from the HOMO of the organic semiconductor (donor) to the LUMO of the transition metal oxides (acceptor), resulting in the formation of radicals. The electrical characteristics of the organic semiconductor-transition metal oxide bilayer showed that there is an enhancement in current and conductivity, which is attributed to the generation of free charges from CTC. The currents measured at 100 V were $1.5 \times 10^{-9}$ A for $MoO_3$/2TNATA, $2.4 \times 10^{-9}$ A for $MoO_3$/NBP, $2.4 \times 10^{-9}$ A for $MoO_3$/TCTA and $7.4 \times 10^{-9}$ A for $MoO_3$/CBP, which are one order greater than that of intrinsic $MoO_3$ having a value of $3.9 \times 10^{-10}$ A. The conductivity of the bilayers was measured

to be $6.2 \times 10^{-6}$ S cm$^{-1}$ for $MoO_3$/2TNATA, $7.7 \times 10^{-6}$ S cm$^{-1}$ for $MoO_3$/NBP, $1.4 \times 10^{-5}$ S cm$^{-1}$ for $MoO_3$/TCTA, and $3.8 \times 10^{-5}$ S cm$^{-1}$ for $MoO_3$/CBP, which was considerably enhanced compared to that of intrinsic $MoO_3$ of $2.6 \times 10^{-6}$ S cm$^{-1}$. On comparing the $MoO_3$/organic semiconductor bilayers, a trend of decreasing conductivity is seen with an increase in CTC density at the interface. This trend was also exhibited by $MoO_3$/NBP, $ReO_3$/NBP and $WO_3$/NBP with conductivity of $7.7 \times 10^{-6}$ S cm$^{-1}$, $1.1 \times 10^{-6}$ S cm$^{-1}$ and $5.2 \times 10^{-6}$ S cm$^{-1}$, respectively. Similar results were also obtained while measuring the activation energy, wherein the interfaces with high CTC densities exhibited hinderance and lower lateral conductivity. Thus, even when the energy difference between the HOMO of the organic semiconductor and LUMO of TMO is large, other factors such as density of CTC in the interface can reduce the conductivity.

Bulk doping has an advantage over contact doping, given that co-evaporation of the dopant/host and not requiring complex patterning make it a much more simpler process.[74] Lee *et al.*[75] demonstrated that bulk doping with high work function metal oxides such as $MoO_3$ and $ReO_3$ as p-type dopants in organic semiconductor materials improved the generation of holes, current density, and conductivity and increased the carrier density and mobilities. The CTC formed in 25 mol% doped 2TNATA improved the electrical conductivities with 25 mol% $ReO_3$ and $MoO_3$, obtaining values of $2 \times 10^{-7}$ and $3.3 \times 10^{-8}$ S cm$^{-1}$, respectively. In the case of doping at the same concentration, the charge transfer complexation increases with an increase in energy difference between the HOMO of the organic semiconductor and Fermi level of the dopant, and thus $ReO_3$ having a higher energy difference shows higher conductivities. Chan *et al.*[76] investigated the effects of transition metal oxides (TMOs) as p-dopants on organic thin film transistors. Doping of the transition metal oxides $MoO_3$, $V_2O_5$ and $WO_3$ in an organic hole transporting semiconductor (NBP) results in the formation of a charge transfer complex and is shown to increase the conductivity of organic thin film transistors, which is attributed to an increase in the free carrier concentration. The electrical characteristics of TMO-doped OTFTs were determined and their *I–V* characteristics showed linearity, indicating the formation of ohmic contact in the transition metal oxide/organic semiconductor interface. The conductivity was measured to be $2.2 \times 10^{-7}$ S cm$^{-1}$ for $MoO_3$-doped NBP, $5.1 \times 10^{-8}$ S cm$^{-1}$ for $WO_3$-doped NBP and $2.8 \times 10^{-8}$ S cm$^{-1}$ for $V_2O_5$-doped NBP, with an increase in conductivity observed with an increase in temperature. A decrease in mobilities was observed in the doped devices compared to the devices with only an NBP layer having linear mobility ($\mu_{lin}$) of $1.1 \times 10^{-5}$ cm$^2$ V$^{-1}$ s$^{-1}$ and saturation mobility ($\mu_{sat}$) of $7.8 \times 10^{-6}$ cm$^2$ V$^{-1}$ s$^{-1}$ to $MoO_3$-doped NBP, $WO_3$-doped NBP and $V_2O_5$-doped NBP having linear mobility ($\mu_{lin}$) and saturation mobility ($\mu_{sat}$) of $5 \times 10^{-6}$ cm$^2$ V$^{-1}$ s$^{-1}$ and $9.4 \times 10^{-6}$ cm$^2$ V$^{-1}$ s$^{-1}$, $4.1 \times 10^{-6}$ cm$^2$ V$^{-1}$ s$^{-1}$ and $5.6 \times 10^{-6}$ cm$^2$ V$^{-1}$ s$^{-1}$, $6.6 \times 10^{-6}$ cm$^2$ V$^{-1}$ s$^{-1}$ and $7.4 \times 10^{-6}$ cm$^2$ V$^{-1}$ s$^{-1}$, respectively. This has been attributed to the presence of anions, which have tendencies to trap holes, briefly causing a reduction in the hole mobilities. The extracted free hole concentration showed an enhancement on doping, with $MoO_3$-doped NBP exhibiting the highest carrier concentration of $1.4 \times 10^{17}$ cm$^{-3}$ compared to $WO_3$ and $V_2O_5$ with values of $5.7 \times 10^{16}$ and $2.4 \times 10^{16}$ cm$^{-3}$, respectively. This is evidence that an increase in carrier concentration causes an enhancement in conductivity, while a decrease in the carrier mobility upon doping is not the reason for enhancement in conductivity. Furthermore, doping with transition metal oxides has also been associated with a lower activation energy, enhancing the carrier generation, with $MoO_3$-doped NBP having $E_a$ of 138 meV, $WO_3$-doped NBP having $E_a$ of 142 meV and $V_2O_5$-doped NBP having $E_a$ of 166 meV. Yedikardes *et al.*[77] investigated the effects of various doping concentrations of $WO_3$ (10–50%) in P3HT to obtain significant OTFT device improvements. Doping concentrations in the range of 0 to 30% $WO_3$ resulted in an increase in the device parameters, reaching the maximum, and then showing a decline in performance with an increase in doping from 30 to 50%. The doping of $WO_3$ on P3HT results in the formation of a charge transfer complex by electron transfer *via* the HOMO of P3HT to the conduction band of $WO_3$, leaving behind mobile holes. This mechanism considerably enhances the field effect mobility, threshold voltage and on/off current ratio. In the case of doping concentrations of 0, 10%, 20%, 30%, 40%, and 50%, the field effect mobility values were $5.3 \times 10^{-5}$, $2.8 \times 10^{-4}$, $5.6 \times 10^{-3}$, $1.1 \times 10^{-3}$ and $9.0 \times 10^{-4}$ cm$^2$ V$^{-1}$ s$^{-1}$, the threshold voltage values were 40.1, 37.2, 17.7, 32.7, and 45.1 V, and the on/off current ratio values were $2.5 \times 10^2$, $5.0 \times 10^2$, $2.3 \times 10^3$, $1.0 \times 10^3$ and $5.0 \times 10^1$, respectively.

Li *et al.*[78] utilized multiparticle Monte Carlo simulations to examine the effects of doping organic semiconductors with transition metal oxides (TMOs). The hole only devices face a major challenge due to the non-uniform electric field caused by the potential barriers at the anode, which is attributed to the lower electric fields near the anode due to space charge perturbation. Thus, the organic devices must be optimized to lower the injection barrier height, which is possible with the help of incorporating high work function transition metal oxides. Doping of the devices with transition metal oxides resulted in a redistribution of charge carriers and electric field, leading to a more uniform electric field, with a higher electric field near the anode compared to the undoped systems, while at the same time doping caused a broader density of state (DOS) distribution, leading to complicated charge mobility behaviour. Hence, the charge mobility is observed to decrease with the doping concentration at low energetic disorders, while at high energetic disorders, the charge mobility first decreases, and then increases with an increase in doping concentration and free charge carriers, while the current densities always increase with doping concentration regardless of the energetic disorder.[79] The Monte Carlo simulations provide insight into the complex mechanisms of charge transport and can validate the results obtained experimentally.

### 3.3 Metal oxides as bilayer electrode layer

The usage of metal oxides in bilayer source–drain (S–D) electrodes in organic thin film transistors has been shown to significantly

enhance the organic device performance in terms of improved charge injection and mobility, high optical transparency, reduced contact resistance, smoother surfaces, improved threshold voltage, subthreshold slope and suppression of the short-channel effect. These bilayer electrodes typically consist of a metal oxide layer paired with a metal, optimizing the interface between the electrode and the organic semiconductor (Fig. 3). Various transition metal oxides (TMOs) have been utilized as bilayer source–drain (S–D) electrode layers owing to their high work function and wide band gap. Fig. 3 describes the resulting device enhancement on incorporating metal oxides as bilayer electrodes by comparing the mechanism of charge injection in metal/organic semiconductor and metal/metal oxide/organic semiconductor configurations. These bilayer metal oxides primarily reduce the barrier height required for charge injection, providing critical tuning of the contact. Thus, inserting a transition metal oxide layer such as $MoO_3$, $V_2O_5$, and $WO_3$ improved the field effect mobilities and on/off current ratios and reduced the contact resistance. These metal oxide layers protect from direct contact in the organic/metal interface, preventing diffusion or any unfavourable chemical reactions.[80]

Alam *et al.*[81] investigated the use of germanium oxide (GeO) and titanium oxide ($TiO_2$)[82] with Au as a bilayer electrode in pentacene top contact organic thin film transistors (OTFTs). GeO/Au as the bilayer electrode in the top-contact OTFTs resulted in a considerable enhancement in field-effect mobility ($\mu$), threshold voltage ($V_T$), and on/off current ratio ($I_{ON}/I_{OFF}$) compared to the devices with only an Au electrode. The devices with 5 nm GeO exhibited the greatest improvement in electrical properties with the field-effect mobility ($\mu$) of 0.96 $cm^2\ V^{-1}\ s^{-1}$, threshold voltage ($V_T$) of −4 V and on/off current ratio ($I_{ON}/I_{OFF}$) of $5.2 \times 10^4$. The root mean square (RMS) roughness for the devices without a GeO layer is 5.94 nm and that with 5 nm GeO is 5.20 nm, indicating smoother surfaces, which are required for improving the ohmic contacts. The valence band of GeO lies below the highest occupied molecular orbital (HOMO) level of pentacene, which reduces the barrier for hole injection into the pentacene layer, facilitating better charge injection and improving the device performance. The GeO layer also protects pentacene from direct contact with the Au electrodes, minimizing Au penetration and preventing unfavourable chemical reactions between the organic and metal layers. The insertion of a titanium oxide ($TiO_2$) layer between the Au electrode and the pentacene layer in an organic thin-film transistor also is shown to improve the device performance by reducing the hole injection barrier and contact resistance at the Au/pentacene interface. The electrical properties measured in devices containing $TiO_2$ were comparatively better than that of the devices without a metal oxide bilayer electrode, exhibiting a field-effect mobility ($\mu$) of 0.63 $cm^2\ V^{-1}\ s^{-1}$, threshold voltage ($V_T$) of −1.5 V, and on/off current ratio ($I_{ON}/I_{OFF}$) of $3.7 \times 10^4$. The alignment of the highest occupied molecular orbital (HOMO) of

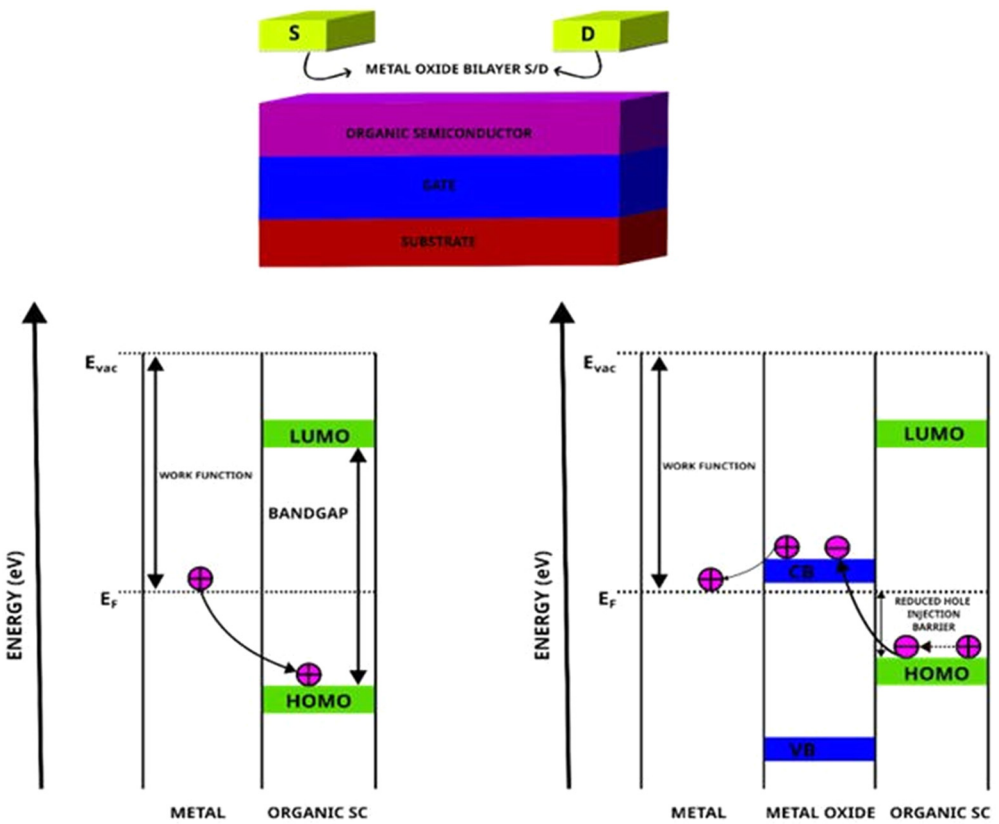


Fig. 3 Schematic representation of metal oxides as bilayer source–drain (S–D) electrodes in an OTFT and schematic comparing the mechanism of charge injection in metal/organic semiconductor and metal/metal oxide/organic semiconductor configurations.

pentacene with the valence band of $TiO_2$ reduces the barrier height for hole injection into the pentacene layer. Without the $TiO_2$ layer, there is a significant hole injection barrier of 0.8–1 eV at the Au/pentacene interface. By inserting the $TiO_2$ layer, this barrier is removed, leading to enhanced charge injection and improved mobility in the OTFTs. Additionally, the $TiO_2$ layer smoothens the surface of the pentacene film. The root mean square (RMS) roughness decreased from 7.45 nm for pentacene alone to 7.05 nm with a 5 nm $TiO_2$ layer. This smoother surface further contributes to lowering the barrier height, increasing charge injection, and ultimately improving the device performance.

Ablat *et al.*[83] studied the role of a metal/metal oxide bilayer electrode in organic field effect transistors (OFETs). Different OFETs were explored having bilayer electrodes with $MoO_3$ and $WO_3$ as metal oxides and Ag and Au as metals. The presence of metal oxides greatly reduces the contact resistance and the metal/metal oxide bilayer electrode showed a considerable increase in the output current of the devices compared to the devices with only Au/Ag metal electrodes. The output characteristics of the metal oxide bilayer exhibited enhanced linearity at low $V_{SD}$. The metal/metal oxide bilayers provided improved threshold voltages, on/off current ratios and subthreshold slopes. The best electrical characteristics were obtained in the devices that used $MoO_3$/Ag bilayer electrodes with a threshold voltage of −14.7 V, on/off current ratio of $5.1 \times 10^6$, and subthreshold slope of 2.4 V $dec^{-1}$. The maximum field effect mobilities ($\mu_{max}$) were found to be 1.35 $cm^2\ V^{-1}\ s^{-1}$ for only Ag, 1.13 $cm^2\ V^{-1}\ s^{-1}$ for $WO_3$/Ag, 1.30 $cm^2\ V^{-1}\ s^{-1}$ for $MoO_3$/Ag, 0.69 $cm^2\ V^{-1}\ s^{-1}$ for only Au, 0.96 $cm^2\ V^{-1}\ s^{-1}$ for $WO_3$/Au, and 0.76 $cm^2\ V^{-1}\ s^{-1}$ $MoO_3$/Au. Although the Ag-only devices gave the highest field effect mobility, it forms the highest contact resistance and largest threshold shift, making it unfavourable compared to the bilayer electrode. The contact resistance values at $V_{GS} = -30$ V were measured to be 860.6 kΩ cm for only Ag, 43 kΩ cm for $WO_3$/Ag, 29.5 kΩ cm for $MoO_3$/Ag, 742 kΩ cm for only Au, 669 kΩ cm for $WO_3$/Au, and 120.5 kΩ cm for $MoO_3$/Au, confirming the reduced contact resistance in the metal/metal oxide bilayer electrodes. Ultraviolet photoelectron spectroscopy (UPS) was used to the study energy level alignment in the bilayer electrode interface and metal-only electrode interface. Bare $C_8$-BTBT has a valence band edge of 2.13 eV below the Fermi level and estimated HOMO of 5.4 eV. In contrast, in the metal oxide bilayer, the valence band edges are at 0.64 eV for $C_8$-BTBT/$MoO_3$ and 1.0 eV for $C_8$-BTBT/$WO_3$, which is in contrast with that found in the literature. This confirms the presence of delocalized gap states that shifts the HOMO of $C_8$-BTBT to 0.64 eV by $MoO_3$ or 1 eV by $WO_3$. Thus, the presence of $MoO_3$ and $WO_3$ interlayers reduces the injection barrier compared to the Ag- or Au-only electrodes. The lower injection barrier with $MoO_3$ explains its superior performance compared to $WO_3$ in OFETs. The study of the surface morphology using AFM demonstrated the impact of the morphology of the interface between the metal/metal oxide bilayers. The larger RMS roughness of $WO_3$ compared to $MoO_3$ results in inhomogeneity, causing large grains and voids. However, the RMS roughness measured for the bilayer electrode shows that the metal can diffuse when in direct contact with the metal oxide and fill the voids. This results in a similar RMS roughness for both $MoO_3$ and $WO_3$ in the bilayer electrode system with metal.

Borthakur *et al.*[84] investigated organic thin film transistors (OTFTs) using a transition metal oxide, $MoO_3$, layer at the organic/electrode interface. The devices with the metal oxide bilayer showed an improved device performance, which was confirmed by the measured field effect mobilities, with the oxidized $MoO_3$/Au bilayer S–D electrode having a field effect mobility of 1.7 $cm^2\ V^{-1}\ S^{-1}$ and laboratory-produced $MoO_3$/Au bilayer S–D electrode having a field effect mobility of 1.03 $cm^2\ V^{-1}\ S^{-1}$ compared to the field effect mobility of 0.18 $cm^2\ V^{-1}\ S^{-1}$ for the Au-only electrode OTFTs. The on/off current ratio of the oxidized $MoO_3$/Au bilayer S–D electrode was obtained to be $2 \times 10^6$ and that of the laboratory-produced $MoO_3$/Au was $2 \times 10^5$, while the threshold voltage of −3.5 V was obtained in the oxidized $MoO_3$/Au bilayer S–D electrodes compared to −1.1 V obtained in the laboratory-produced $MoO_3$/Au. Thus, the oxidized $MoO_3$/Au bilayer S–D electrode was shown to have a better field effect mobility, on/off current ratio and threshold voltage compared to the laboratory-produced $MoO_3$/Au bilayer S–D electrode, inferring that the combination of molybdenum oxides ranging from $MoO_3$ to MoO as well as a small amount Mo can provide a better interface compared to pure $MoO_3$. Similar enhancements in OTFT device performance was obtained when a $V_2O_5$/Au bilayer electrode was employed.[85] The $V_2O_5$/Au devices obtained a field effect mobility of 0.77 $cm^2\ V^{-1}\ s^{-1}$ compared to the bare Au device with a value of 0.18 $cm^2\ V^{-1}\ s^{-1}$. The threshold voltage and on/off current ratio also showed comparable improvements, with the bilayer source–drain devices obtaining values of −2.9 V and $7.5 \times 10^5$, while the bare Au electrode device obtained −1.2 V and $7.5 \times 10^4$, respectively. Thus, efficient OTFT devices could be realised by the application of metal oxides in a bilayer electrode system through reduced contact resistance and injection barrier.

The practical application of metal oxides towards engineering better organic electronics can pave way for superior performances. Developments in OTFT sensor applications have incorporated the use of metal oxide interlayers for enhanced performance. Jain *et al.*[86] investigated the use of a bilayer electrode in a dielectric-modulated OTFT biosensor to obtain high performances. A bilayer electrode system of Au (20 nm)/$TiO_2$ (5 nm) provides significant reductions in injection barrier, providing an enhanced on/off current ratio. The bilayer electrode interface provides enhanced sensitivity, which is an operation critical for any sensor application. The dielectric-modulated bilayer electrode OTFT biosensor achieved a significantly enhanced device performance in terms of sensitivity, achieving a drain current sensitivity of 50.91.

### 3.4 Metal oxides as gate dielectrics

Low-voltage operation in organic thin film transistors is a desirable trait, which can be attained at high capacitance by either reducing the dielectric thickness or increasing the

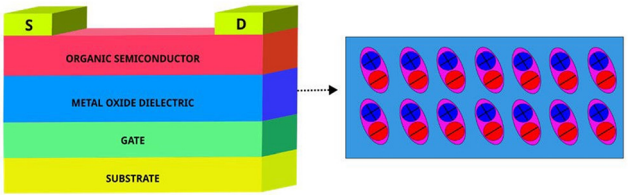


Fig. 4 Schematic representation of a metal oxide gate dielectric in an OTFT.



dielectric constant. Metal oxides such as aluminium oxide ($Al_2O_3$), hafnium oxide ($HfO_2$), zirconium oxide ($ZrO_2$) and rare earth metal oxides such as neodymium oxides ($Nd_2O_3$) and lanthanum oxides ($La_2O_3$) offer much higher dielectric constants compared to the commonly used silicon oxides ($SiO_2$), thus achieving greater capacitance values. Compared to $SiO_2$, metal oxides serve as promising gate dielectric materials for organic thin film transistors due to their high dielectric constants, relatively high bandgap, high mechanical stability, and high electric field strength. Fig. 4 shows a schematic representation of a metal oxide gate dielectric in OTFT. Metal oxides are used in OTFTs to achieve low voltage operation, high operational stability, smooth surfaces, optimized surface modification, high current on/off ratio, low subthreshold swing, and suppressed current leakage.

One of the major drawbacks associated with utilising inorganic metal oxides as gate dielectrics in OTFTs is the requirement of expensive and sophisticated instruments for deposition including high-vacuum processes such as sputtering, atomic layer deposition and vacuum evaporation, high-temperature annealing processes and anodized processes. Hence, there is a need for alternative methods as low-cost and efficient deposition techniques. Byun *et al.*[87] employed a simple and cost-effective sol–gel method to fabricate high dielectric UV curable hafnium oxide ($HfO_x$) compared to thermally annealed $HfO_x$. Phosphonic acid-based *n*-dodecylphosphonic acid (C12PA) served as a self-assembled monolayer (SAM), functioning to optimize the surface energy for enhanced crystallization of the organic semiconductor as well as enhance the device performance by increasing the leakage barrier. The morphological study of the dielectric layer by atomic force microscopy provided insights into the smooth surfaces obtained for both processing methods, with the maximum RMS roughness of 0.3 nm. Although UV-cured $HfO_x$ provides an alternative to high temperature processes, a trade-off resulting in lower dielectric properties is seen. Excellent OTFT device parameters were obtained with the UV-cured $HfO_x$ dielectric along with pentacene organic semiconductors, with the capacitance of 540 nF $cm^{-2}$, leakage current of $7.2 \times 10^{-7}$ A $cm^{-2}$, hole mobility of 0.31 $cm^2$ $V^{-1}$ $s^{-1}$, on/off current ratio of $10^5$, threshold voltage of −0.3 V and low operating voltage of −3 V. Gong *et al.*[88] utilised the solution-processed, low-temperature deposition of UV-cured zirconium oxide ($ZrO_2$) as well as post-deposition thermal annealing (PDA) and compared the different techniques. The thickness of the films prepared by PDA was larger than that of the UV-cured films, confirming that the UV-cured films exhibited better densification. Low-temperature UV-cure processing showed comparable dielectric properties with the leakage current density, capacitance, and dielectric constant of $1.8 \times 10^{-6}$ A $cm^{-2}$, 116 nF $cm^{-2}$, and 8.7 for the UV-irradiated device (exposed for 60 min) compared to that of $3.6 \times 10^{-5}$ A $cm^{-2}$, 261 nF $cm^{-2}$, and 17.8 for the films thermally annealed at 160 °C, respectively. Additionally, the UV-cured device achieved a high performance with the field effect mobility of 0.88 $cm^2$ $V^{-1}$ $s^{-1}$, threshold voltage of −1.16 V and high on/off current ratio of $3.1 \times 10^6$. Zhao *et al.*[89] fabricated low-temperature, solution-based processed UV-cured lanthanum oxide ($La_2O_3$) as a gate dielectric in OTFTs. Thermal annealing of the films at the extremely high temperature of 500 °C caused the films to become polycrystalline, making them thinner compared to the amorphous UV-irradiated films. Although the UV-irradiated films possessed a thickness three-times that of the film prepared *via* the high-temperature process, the amorphous films provide better mechanical flexibility, smoother surfaces and electrical insulation stability, as well as allow for large-scale fabrication on flexible substrates. Moreover, these UV-lanthanum oxide dielectrics possess a large band gap (5.78 eV), high breakdown electric field (>3 MV $cm^{-1}$) and high dielectric constant of 12.68. Excellent OTFT device parameters were obtained with UV-treated $La_2O_3$ with a thin PαMS polymer as an interface modification layer, obtaining the low-voltage operation of below ±3 V for both n-type (PTCDI-C8) and p-type (pentacene) OTFTs, low threshold voltage of −2.368 V and 0.579 V, field effect mobility of 0.815 $cm^2$ $V^{-1}$ $s^{-1}$ and 0.026 $cm^2$ $V^{-1}$ $s^{-1}$ and subthreshold slope of 122.9 and 68.8 mV $dec^{-1}$ for n-type and p-type, respectively.

Although the solution processing of metal oxides *via* methods such as sol–gel-based methods makes their processing easier, it commonly involves the use of toxic precursors and solvents that harm the environment. Thus, there is a growing need for green processing methods to comply with sustainability. Dacha *et al.*[90] investigated ultrathin DUV-cured and thermal-annealed aluminium oxide ($AlO_x$) films owing to their cost-efficient and eco-friendly qualities. Given that they are derived from non-toxic precursors, aluminium nitrate nonahydrate and utilising green solvents such as water, this method helps promote sustainable electronic manufacturing processes. Ultra-thin films of aluminium oxides ($AlO_x$) of 7 nm fabricated by solution shearing serve as a dielectric layer, making it possible to achieve high capacitance values of 750 nF $cm^{-2}$ and 600 nF $cm^{-2}$ and leakage current of $10^{-6}$ and $10^{-7}$ for the thermal-annealed and UV-cured processes, respectively. The DUV films showed excellent smoothness with a low RMS roughness of 89.4 pm compared to 423.3 pm for the thermal-annealed films. The organic devices are capable of low operation voltage at −0.5 V and obtained a field effect mobility of 6.1 $cm^2$ $V^{-1}$ $s^{-1}$, threshold voltage of −0.14 V and subthreshold slope of 96 mV $dec^{-1}$. Kumar *et al.*[91] investigated a novel water-processed bilayer dielectric to provide an eco-friendly solution for preventing the use of toxic organic solvents. A water-induced

bilayer dielectric of $LiO_x/AlO_x$ in an OTFT of DPP-DTT transferred using the floating film transfer method achieved low-voltage operation with an enhanced device performance. The $LiO_x/AlO_x$ dielectric had a dielectric constant of 7.2 at 1 kHz and capacitance density of 378 ($\pm$ 24) nF cm$^{-2}$. The device metrics showed that the OTFT obtained the mobility of 0.34 cm$^2$ V$^{-1}$ s$^{-1}$, on/off current ratio of $10^5$, subthreshold slope of 90 mV decade$^{-1}$ and threshold voltage of $-0.26$ V.

Barium titanate has emerged as a metal oxide gate dielectric owing to its low cost, biocompatibility, ferroelectric properties and applications due to its temperature sensitivity, providing an excellent performance. Wang *et al.*[92] studied the use of barium titanate as an effective gate dielectric in OTFTs. The surface roughness of the BTO films could be tailored by deposition at room temperature without post-deposition annealing or utilising both deposition and post-deposition annealing at high temperature. The amorphous barium titanate deposited by sputtering at 200 °C without post-deposition annealing achieved a hysteresis-free, high performance with a dielectric constant of 0.36 μF cm$^{-2}$ at 1 MHz. The device showed an excellent device performance with mobility of 2.91 cm$^2$ V$^{-1}$ s$^{-1}$, on/off current ratio of $1.16 \times 10^6$, negligible hysteresis of 18 mV, subthreshold slope of 0.140 V decade$^{-1}$ and threshold voltage of $-1.09$ V. The temperature-sensitive nature of barium titanate could be exploited for sensor applications. Mandal *et al.*[93] utilised low temperature-processed hexagonal barium titanate nanocrystals (h-BTNC) as a gate dielectric, which showed extremely high temperature precision of 4.3 mK and response time of 24 ms, while consuming 1 μW at 1.2 V for a stable and flexible OTFT temperature sensor. The h-BTNC films reduced the surface roughness of $Al_2O_3$ from 3.87 to 0.4, significantly improving the interface for pentacene. The OTFT device parameters were field effect mobility of 1.46 cm$^2$ V$^{-1}$ s$^{-1}$, on/off current ratio of $10^3$ and threshold voltage of $-1.05$ V. The applicability of the devices for commercial scale was also possible by screen printing of the dielectric, obtaining parameters of field effect mobility, threshold voltage and on/off current ratio of 0.70 cm$^2$ V$^{-1}$ s$^{-1}$, $-1.26$ V and $10^3$, respectively.

The use of bilayer dielectrics has been studied to obtain smoother surfaces to improve the interface between the semiconductor and dielectric. These bilayer dielectrics also help tune the electronic properties of OTFTs, especially their threshold voltage. Kim *et al.*[94] explored the use of $HfO_2$ in a bilayer gate dielectric as a means of achieving high operational stability and low threshold voltage in organic thin film transistors. Thin films of $HfO_2$/CYTOP can be achieved in bottom gate-configured organic thin film transistors to obtain a high gate capacitance density value of 276 nF cm$^{-2}$ for BG OTFT. The threshold voltage in the $HfO_2$/CYTOP bilayer gate dielectric devices was measured to be below 1 V, showing a low operational voltage. The electrical parameters showed average values such as field effect mobility measured to be in the range of 0.3–0.8 cm$^2$/V s and subthreshold slope as low as 95 mV dec$^{-1}$. The major advantage of using metal oxide/organic semiconductor bilayer gate dielectrics is the ability to achieve high operational stability for prolonged periods. The operational stability was studied for the devices with the gate bilayer dielectric of $HfO_2$ (20 nm)/CYTOP (5 nm), $HfO_2$ (20 nm)/CYTOP (7 nm) and $HfO_2$ (10 nm)/CYTOP (7 nm). Among them, the best operational stability was obtained with $HfO_2$ (10 nm)/CYTOP (7 nm) bilayer gate dielectric with a change in the drain-to-source current ($|\Delta I_{DS}(t)|$) value of 9% and threshold voltage shift ($|\Delta V_{TH}|$) of 0.1 V observed after 24 h, thereby showing high operational stabilities in OTFTs.

Khound *et al.*[95] studied the use of high $\kappa$ dielectrics rare earth metal oxides such as neodymium oxide ($Nd_2O_3$) and lanthanum oxide ($La_2O_3$) as bilayer gate dielectrics in organic thin film transistors (OTFTs). Pentacene organic thin film transistors were fabricated with an $La_2O_3/Nd_2O_3$ bilayer gate dielectric. These $La_2O_3$ (118 nm)/$Nd_2O_3$ (100, 150, 175 nm) bilayer gate dielectrics were shown to reduce the current leakage compared to the $La_2O_3$-only gate dielectric, given that the addition of $Nd_2O_3$ to $La_2O_3$ smoothens the surface. The root mean square (RMS) value obtained from atomic force microscopy (AFM) was 1.82 nm for the first layer and 0.94 nm for the second layer. The addition of $Nd_2O_3$ to $La_2O_3$ caused the bilayer gate dielectric layer to reduce the threshold voltage to $-1.1$ V compared to $-0.42$ V for the $La_2O_3$-only gate dielectric, providing low operational voltages. The $La_2O_3/Nd_2O_3$ bilayer gate dielectric employed helped the improve electrical properties of OTFTs with $La_2O_3$ (118 nm)/$Nd_2O_3$ (150 nm), showing the best capacitance per unit area ($C_i$) of 28.45 nF cm$^{-2}$, current on/off ratio ($I_{ON}/I_{OFF}$) of $2.4 \times 10^5$, subthreshold slope (SS) of 0.5 V decade$^{-1}$ and carrier mobility of 1.08 cm$^2$ V$^{-1}$ s$^{-1}$.

Recent advancements in organic–inorganic dielectric layers as potential high-quality dielectric films have resulted in high sensitivity, low leakage current and enhanced stability. Although inorganic metal oxides can attain excellent dielectric properties, their application is hindered by their high-temperature processability and lower mechanical stability compared to organic dielectrics. Thus, a hybrid organic–inorganic dielectric can be used to obtain the best of both worlds, with the organic layer exhibiting mechanical flexibility, while high dielectric constants of inorganic layer provide a reduced leakage current. Gallegos-Rosas *et al.*[96] reported the use of mixed metal oxides as a possible solution to achieve high-capacitance dielectric layers in organic light emitting transistors. Hafnium aluminate ($HfAlO_x$) was obtained by $HfO_2$ and $Al_2O_3$ and it showed excellent dielectric properties operational even under low voltage conditions. Reducing the thickness of the gate dielectric layer or using materials having large dielectric constants ($\kappa$) are two important methods to obtain high capacitance dielectrics. However, although polymeric dielectrics are attractive options given that they allow fabrication on plastic substrates, they are constrained due to their low-$\kappa$ values, and thus an alternative approach of organic–inorganic dielectric layer was explored. The $\kappa$ for a hafnium aluminate ($HfAlO_x$)/PMMA bilayer stack at 1 kHz was measured to be 7.1 compared to that of 3.3 for the devices containing PMMA as the dielectric. The hafnium aluminate ($HfAlO_x$) bilayer stack was operational even at low voltages, with a higher capacitance of 63 nF cm$^{-2}$ for the bilayer dielectric compared to 6.6 nF cm$^{-2}$

for PMMA, while exhibiting no dielectric breakdown up to 20 V. The transfer characteristics presented a V shape, indicating that the OLET operated in an ambipolar regime. The hole mobility of the $HfAlO_x$ bilayer was measured to be 1.09 $cm^2\ V^{-1}\ s^{-1}$ compared to that of 0.19 $cm^2\ V^{-1}\ s^{-1}$ for a single PMMA layer, and the electron mobility of the bilayer was obtained to be 0.08 $cm^2\ V^{-1}\ s^{-1}$ compared to 0.003 $cm^2\ V^{-1}\ s^{-1}$ for PMMA. Thus, the bilayer of hafnium aluminate ($HfAlO_x$)/PMMA provided an effective dielectric layer with efficient power consumption and enhanced interface between the organic material and dielectric layers. Priya *et al.*[97] studied the use of high $\kappa$ metal oxides such as $AlO_x$, $TiO_x$ and $TaO_x$ with poly vinyl phenol (PVP) as organic–inorganic dielectrics in OTFTs. The use of metal oxides in the PVP layer considerably improved the smoothness with a surface roughness of 0.33 nm obtained for $AlO_x$, 3.04 nm for $TaO_x$, and 3.74 nm for $TiO_x$. This improvement in smoothness led to improved uniformity in the films, providing an enhanced device performance. The electrical parameters of the device showed the high performance of the OTFT with a mobility of 1.3 $cm^2\ V^{-1}\ s^{-1}$ for the $AlO_x$/PVP dielectric, 1.5 $cm^2\ V^{-1}\ s^{-1}$ for $TiO_x$/PVP and 1.1 $cm^2\ V^{-1}\ s^{-1}$ for $TaO_x$/PVP. The enhancement could be attributed to the similar surface energies of pentacene and PVP, obtaining an optimized arrangement during crystallization, and thus providing an improved interface with the dielectric. Alternatively, the lower relative performance of $TaO_x$/PVP was due to the larger thickness of the $TaO_x$ film reducing the charge transport. The capacitance values of the organic/inorganic films were $1.5 \times 10^{-7}$ F $cm^{-2}$ for $AlO_x$/PVP, $1.9 \times 10^{-7}$ F $cm^{-2}$ for $TiO_x$/PVP, and $2.7 \times 10^{-7}$ F $cm^{-2}$ for $TaO_x$/PVP, providing low voltage application and reduction in leakage current. Although the metal oxide-organic hybrid proved to be an efficient dielectric layer, the high-temperature processing of metal oxides is still an obstacle. Thus, low temperature-based metal oxide nanoparticles can be used to mitigate the limitation of high temperature processing. Le *et al.*[98] prepared low-temperature $TiO_2$ nanoparticles to be used in an amphiphilic polymer as an organic–inorganic dielectric. Amphiphilic urethane polymer (AUP) served as a stabilizing agent for the colloidal $TiO_2$ nanoparticles, providing a mechanically flexible Uti (urethane–$TiO_2$) dielectric. The UTi films were highly uniform, while the $TiO_2$/poly(AUP) nanocomposite films were uneven and non-uniform due to the agglomeration of the metal oxide

Table 1 OTFT device parameters utilising different metal oxides

| Organic semiconductor | Metal oxide | Mobility ($cm^2\ V^{-1}\ s^{-1}$) | Subthreshold slope (V $decade^{-1}$) | Threshold voltage (V) | On/off ratio | Year[Ref.] |
|---|---|---|---|---|---|---|
| Ph-BTBT-10 | $MoO_3$ | 7.9 ($\mu_{FET}$) | N/A | −0.03 | N/A | 2024[6] |
| Pentacene | $MoO_3$ | 0.184 ($\mu_{FET}$) | 5 ± 0.4 | N/A | N/A | 2014[32] |
| Pentacene | $WO_3$ | 0.025 ($\mu_{carrier}$) | N/A | N/A | N/A | 2019[34] |
| Pentacene | $VO_x$ | 0.80 ($\mu_{FET}$) | N/A | N/A | $4 \times 10^5$ | 2016[35] |
| BOPAnt | $VO_x$ | 1.56 ($\mu_{FET}$) | N/A | N/A | $5.6 \times 10^7$ | |
| $C_8$-BTBT | $MoO_3$ | 13.1 ($\mu_{FET}$) | N/A | N/A | N/A | 2018[36] |
| | $V_2O_5$ | 11.6 ($\mu_{FET}$) | N/A | N/A | N/A | |
| | $WO_3$ | 10 ($\mu_{FET}$) | N/A | N/A | N/A | |
| P3HT | ZnO | $2 \times 10^{-3}$ ($\mu_{FET}$) | 6.25 | 10 | 73 | 2023[37] |
| Pentacene | CuO | 0.182 ($\mu_{FET}$) | N/A | −8 | $1.37 \times 10^{-4}$ | 2019[39] |
| Pentacene | CuO | 0.011 ($\mu_{FET}$) | N/A | 7.91 | $10^4$ | 2009[41] |
| TIPS-pentacene | $ReO_3$ | 0.7 ($\mu_h$) | N/A | 0.9 | N/A | 2019[43] |
| $C_8$-BTBT | $MoO_x$ | 2.3 ($\mu_{FET}$) | 0.22 | N/A | N/A | 2009[57] |
| DBTTT | $MoO_x$ | 7.3 ($\mu_{FET}$) | N/A | N/A | N/A | 2017[58] |
| P3HT | $MoO_3$ | $2.1 \times 10^{-2}$ ($\mu_{carrier}$) | N/A | N/A | N/A | 2016[59] |
| | $V_2O_5$ | $0.9 \times 10^{-2}$ ($\mu_{carrier}$) | N/A | N/A | N/A | |
| CuPc | $MoO_3$/NBP (OBL) | $2.74 \times 10^{-4}$ ($\mu_{FET}$) | N/A | 1.98 | $3.72 \times 10^3$ | 2023[64] |
| Polythiophene | $MoO_x$ | N/A | 1 | −4.5 | N/A | 2025[66] |
| Pentacene | $MoO_3$ | 1.40 ($\mu_{FET}$) | −4.54 | −13.8 | $10^5$ | 2018[67] |
| Pentacene | $MoO_3$ | $1.71 \times 10^{-1}$ ($\mu_h$) | N/A | −16.69 | $2.5 \times 10^3$ | 2025[68] |
| Pentacene | $MoO_3$ | 0.36 ($\mu_h$) | N/A | −33.7 | N/A | 2014[69] |
| m-MTDATA | | 0.40 ($\mu_h$) | N/A | −20.7 | N/A | |
| Pentacene/m-MTDATA | | 0.72 ($\mu_h$) | N/A | −13.4 | $10^2$ | |
| Pentacene | $WO_3$/m-MTDATA (CTC) | $2.69 \times 10^{-2}$ ($\mu_{FET}$) | N/A | −0.0054 | N/A | 2020[70] |
| CuPc/F16CuPc | $V_2O_5$/2T-NATA (CTC) | $6.6 \times 10^{-5}$ ($\mu_{FET}$) | N/A | N/A | N/A | 2023[71] |
| | | $7.18 \times 10^{-5}$ ($\mu_{FET}$) | N/A | N/A | N/A | |
| NBP | $MoO_3$ | $9.4 \times 10^{-6}$ ($\mu_{FET}$) | N/A | N/A | N/A | 2011[76] |
| | $V_2O_5$ | $7.4 \times 10^{-6}$ ($\mu_{FET}$) | N/A | N/A | N/A | |
| | $WO_3$ | $5.6 \times 10^{-6}$ ($\mu_{FET}$) | N/A | N/A | N/A | |
| P3HT | $WO_3$ | $5.6 \times 10^{-3}$ ($\mu_{FET}$) | N/A | 17.7 | $2.3 \times 10^3$ | 2020[77] |
| Pentacene | $MoO_3$ | 0.4 ($\mu_{FET}$) | N/A | −12.1 | $3.8 \times 10^4$ | 2005[80] |
| | $V_2O_5$ | 0.226 ($\mu_{FET}$) | N/A | −10.43 | $1.8 \times 10^4$ | |
| | $WO_3$ | 0.253 ($\mu_{FET}$) | N/A | −12.88 | $4.1 \times 10^4$ | |
| Pentacene | GeO | 0.96 ($\mu_{FET}$) | N/A | −4 | $5.2 \times 10^4$ | 2013[81] |
| Pentacene | $TiO_2$ | 0.63 ($\mu_{FET}$) | N/A | −1.5 | $3.7 \times 10^4$ | 2012[82] |
| $C_8$-BTBT | $MoO_3$ | 1.30 ($\mu_{FET}$) | 1.7 | −14.7 | $5.1 \times 10^6$ | 2019[83] |
| | $WO_3$ | 1.13 ($\mu_{FET}$) | 1.9 | −17.8 | $8.2 \times 10^5$ | |
| Pentacene | $MoO_3$ | 1.7 ($\mu_{FET}$) | 0.39 | −3.5 | $2.5 \times 10^6$ | 2022[84] |
| Pentacene | $V_2O_5$ | 0.77 ($\mu_{FET}$) | 0.36 | −2.9 | $7.5 \times 10^5$ | 2017[85] |

Table 2 Properties of different metal oxide gate dielectrics

| Organic semiconductor | Metal oxide | Leakage current density (A $cm^{-2}$) | Capacitance (nF $cm^{-2}$) | Dielectric constant | Year[Ref.] |
|---|---|---|---|---|---|
| Pentacene | $ZrO_2$ | $1.89 \times 10^{-6}$ | N/A | 19.70 | 2016[45] |
| FS11 | $HfO_2$ | $10^{-7}$ | N/A | 26 | 2014[46] |
| DNTT | $AlO_x$ | $10^{-6}$ | 700 | | 2021[47] |
| Pentacene | NdNbON | N/A | N/A | 8.5 | 2022[48] |
| Pentacene | $La_2O_3$/cPVP | N/A | 65 | 9.2 | 2022[49] |
| | $La_2O_3$ | N/A | 50.4 | 7.2 | |
| Pentacene | $ZrO_x$ | $8 \times 10^{-8}$ | 188 | 15 | 2018[50] |
| Pentacene | $ZrO_2$/PI | $7.32 \times 10^{-9}$ | N/A | 8.1 | 2017[51] |
| Pentacene | $PrO_x$ | N/A | 290 | 13 | 2023[52] |
| | $SmO_x$ | N/A | 390 | 22 | |
| | $GdO_x$ | N/A | 880 | 11.5 | |
| | $TbO_x$ | N/A | 600 | 15.1 | |
| | $ErO_x$ | N/A | 580 | 14.1 | |
| | $YbO_x$ | N/A | 1900 | 13.5 | |
| Pentacene | $HfO_x$ | $7.2 \times 10^{-7}$ | 540 | | 2019[87] |
| Pentacene | $ZrO_x$ | $1.8 \times 10^{-6}$ | 261 | 17.8 | 2018[88] |
| Pentacene | $La_2O_3$ | $8.8 \times 10^{-7}$ | N/A | 12.68 | 2019[89] |
| PTCDI-C8 | | | | | |
| C10-DNTT | $AlO_x$ | $10^{-6}$ | 750 | N/A | 2024[90] |
| DPP-DTT | $LiO_x$/$AlO_x$ | $2.5 \times 10^{-9}$ | 378 ($\pm$ 24) | 7.2 | 2023[91] |
| | $LiO_x$ | $3.7 \times 10^{-8}$ | 195 ($\pm$ 15) | 7.94 | |
| Pentacene | a-BTO | $9.75 \times 10^{-8}$ | 360 | 7.87 | 2024[92] |
| Pentacene | h-BTNC/$Al_2O_3$ | N/A | 158 | N/A | 2019[93] |
| DPP-DTT | $HfO_2$/CYTOP | N/A | 276 | N/A | 2020[94] |
| Pentacene | $La_2O_3$/$Nd_2O_3$ | $10^{-7}$ | 28.45 | N/A | 2019[95] |
| $C_8$-BTBT | $HfAlO_x$ | N/A | 63 | 7.1 | 2024[96] |
| DFH-4T | | | | | |
| Pentacene | $AlO_x$/PVP | N/A | 150 | N/A | 2024[97] |
| | $TiO_x$/PVP | N/A | 190 | N/A | |
| | $TaO_x$/PVP | N/A | 270 | N/A | |
| C10-DNTT | $TiO_2$/poly(AUP) | $2.6 \times 10^{-7}$ | 50 | 18.6 | 2024[98] |

nanoparticles. The UTi films exhibited dielectric constants as high as 18.9 at 1 MHz, providing a reduced leakage current of $2.6 \times 10^{-7}$ at 2 MV $cm^{-1}$ with the shortest hydrophilic polyethylene oxide chain (molecular weight of 550 g $mol^{-1}$). This was largely due to the better packing obtained with shorter hydrophilic PEO chains, while longer chains are more prone to aggregation. The OTFT performance of UTi-m550 exhibited the average effective field-effective mobility of 6.39 $cm^2 V^{-1} s^{-1}$, on/off current ratio of $1.76 \times 10^4$, subthreshold slope of 0.272 V $dec^{-1}$ and threshold voltage of $-0.95$ V (Tables 1 and 2).

## 4. Conclusion

Metal oxides have emerged as versatile and effective components to enhance the performance of organic thin-film transistors (OTFTs). Their incorporation as hole injection layers significantly lowers the hole injection barrier, leading to improved carrier mobility and reduced contact resistance. The formation of charge transfer complexes (CTCs) at the metal oxide/organic semiconductor interface further optimizes the energy level alignment, facilitating efficient charge transfer. Additionally, when employed as part of bilayer source–drain electrodes, metal oxides not only provide enhanced field-effect mobility, on/off current ratios, smoother surfaces, and improved threshold voltages and subthreshold slopes but also offer crucial protection against undesirable chemical reactions at the interface between the metal/organic semiconductor. Metal oxides play an important role as gate dielectrics, contributing to high capacitance, dielectric constant, potential for low temperature and solution processability, and electrical and mechanical stability.

However, despite these advancements, organic thin film transistors are inferior to silicon-based transistors owing to their inconsistent physical models, lower charge carrier mobilities, higher contact resistance, diffusion at the interfaces, reproducibility and reduced environmental stability. The deposition of metal oxides requires high cost and sophisticated instruments, hindering their large-scale production. Nevertheless, organic thin film transistors can play a critical part in next-generation organic electronics, emerging as inexpensive, flexible, lightweight, biocompatible, low temperature-processible and solution-processible alternatives to silicon-based technology, and utilized in various applications including flexible displays, wearable devices, radio frequency identification tags (RFID), shelf tags, e-skin, biosensors, bio-implantable devices and flexible integrated circuits.

As research progresses, optimized materials and device architectures will drive the next generation of organic electronics, meeting the growing demand for high-performance, energy-efficient, and sustainable technologies.

## Author contributions

Conceptualization: Poornima Bhagavath; methodology: Nikhil Pais, Manav Jeetendra Shirodkar and Poornima Bhagavath; formal analysis: Nikhil Pais, Manav Jeetendra Shirodkar and Poornima Bhagavath; investigation: Nikhil Pais, Manav

Jeetendra Shirodkar; writing – original draft: Nikhil Pais, Manav Jeetendra Shirodkar and Poornima Bhagavath; writing – review & editing: Nikhil Pais, Manav Jeetendra Shirodkar and Poornima Bhagavath; funding acquisition: Poornima Bhagavath; resources: Poornima Bhagavath; supervision: Poornima Bhagavath.

## Conflicts of interest

There are no conflicts to declare.

## Data availability

No primary research results, software or code have been included and no new data were generated or analysed as part of this review.

## Acknowledgements

We thank Manipal Institute of Technology and Manipal Academy of Higher Education for providing the necessary facilities to pursue this review work with renewed vigor.

## References

1 T. Minamiki, *et al.*, Flexible organic thin-film transistor immunosensor printed on a one-micron-thick film, *Commun. Mater.*, 2021, **2**(1), 1–8, DOI: **10.1038/s43246-020-00112-z**.
2 R. A. Nawrocki, N. Matsuhisa, T. Yokota and T. Someya, 300-nm Imperceptible, Ultraflexible, and Biocompatible e-Skin Fit with Tactile Sensors and Organic Transistors, *Adv. Electron. Mater.*, 2016, **2**(4), 1500452, DOI: **10.1002/aelm.201500452**.
3 N. Wang, A. Yang, Y. Fu, Y. Li and F. Yan, Functionalized Organic Thin Film Transistors for Biosensing, *Acc. Chem. Res.*, 2019, **52**(2), 277–287, DOI: **10.1021/acs.accounts.8b00448**.
4 C. B. Park, K. M. Kim, J. E. Lee, H. Na, S. S. Yoo and M. S. Yang, Flexible electrophoretic display driven by solution-processed organic TFT with highly stable bending feature, *Org. Electron.*, 2014, **15**(12), 3538–3545, DOI: **10.1016/j.orgel.2014.09.039**.
5 M. Yamada, Y. Takeda, S. Tokito and H. Matsui, Printed organic transistors and complementary ring oscillators operatable at 200 mV, *Appl. Phys. Express*, 2024, **17**(1), 011010, DOI: **10.35848/1882-0786/ad1db5**.
6 T. J. Mun, J. Kim, J. Seong, Y. Jang, W. Lee and H. Seong, Large-Area Processable Ultrathin Organic Transistors with High Mobility and Mechanical Stabilities, *Adv. Electron. Mater.*, 2024, **10**(7), 2300800, DOI: **10.1002/aelm.202300800**.
7 S. Duan, *et al.*, Scalable Fabrication of Highly Crystalline Organic Semiconductor Thin Film by Channel-Restricted Screen Printing toward the Low-Cost Fabrication of High-Performance Transistor Arrays, *Adv. Mater.*, 2019, **31**(16), 1807975, DOI: **10.1002/adma.201807975**.
8 M. Mizukami, *et al.*, Flexible Organic Light-Emitting Diode Displays Driven by Inkjet-Printed High-Mobility Organic Thin-Film Transistors, *IEEE Electron Device Lett.*, 2018, **39**(1), 39–42, DOI: **10.1109/LED.2017.2776296**.
9 Y. Zang, F. Zhang, D. Huang, X. Gao, C. Di and D. Zhu, Flexible suspended gate organic thin-film transistors for ultra-sensitive pressure detection, *Nat. Commun.*, 2015, **6**(1), 6269, DOI: **10.1038/ncomms7269**.
10 V. Fiore, *et al.*, An Integrated 13.56-MHz RFID Tag in a Printed Organic Complementary TFT Technology on Flexible Substrate, *IEEE Trans. Circuits Syst. Regul. Pap.*, 2015, **62**(6), 1668–1677, DOI: **10.1109/TCSI.2015.2415175**.
11 S. Lai, *et al.*, Optimization of organic field-effect transistor-based mechanical sensors to anisotropic and isotropic deformation detection for wearable and e-skin applications, *Sens. Actuators, A*, 2024, **368**, 115101, DOI: **10.1016/j.sna.2024.115101**.
12 S. Bhandari, T. D. Dhamale, R. K. Kawade, D. N. Dhake and G. Wadhwa, Dielectric modulated organic thin film transistor trench biosensor for label-free detection: Modeling and simulation analysis, *Int. J. Numer. Model. Electron. Netw. Devices Fields*, 2024, **37**(2), e3186, DOI: **10.1002/jnm.3186**.
13 Y. Takeda, *et al.*, Fabrication of Ultra-Thin Printed Organic TFT CMOS Logic Circuits Optimized for Low-Voltage Wearable Sensor Applications, *Sci. Rep.*, 2016, **6**(1), 25714, DOI: **10.1038/srep25714**.
14 U. Zschieschang, *et al.*, Flexible low-voltage organic thin-film transistors and circuits based on C10-DNTT, *J. Mater. Chem.*, 2012, **22**(10), 4273–4277, DOI: **10.1039/C1JM14917B**.
15 C.-L. Fan, W.-C. Lin, H.-S. Chang, Y.-Z. Lin and B.-R. Huang, Effects of the F4TCNQ-Doped Pentacene Interlayers on Performance Improvement of Top-Contact Pentacene-Based Organic Thin-Film Transistors, *Materials*, 2016, **9**(1), 46, DOI: **10.3390/ma9010046**.
16 S. Nagamatsu and S. S. Pandey, Ordered arrangement of F4TCNQ anions in three-dimensionally oriented P3HT thin films, *Sci. Rep.*, 2020, **10**(1), 20020, DOI: **10.1038/s41598-020-77022-0**.
17 S. Gilioli, *et al.*, Charge-Transfer Complexes: Halogen-Doped Anthracene as a Case of Study, *Chem. – Eur. J.*, 2024, **30**(41), e202400519, DOI: **10.1002/chem.202400519**.
18 R. Abdur, K. Jeong, M. J. Lee and J. Lee, High performance of pentacene organic thin film transistors by doping of iodine on source/drain regions, *Org. Electron.*, 2013, **14**(4), 1142–1148, DOI: **10.1016/j.orgel.2013.02.001**.
19 Y. Han, *et al.*, Doping of Large Ionization Potential Indenopyrazine Polymers *via* Lewis Acid Complexation with Tris(pentafluorophenyl)borane: A Simple Method for Improving the Performance of Organic Thin-Film Transistors, *Chem. Mater.*, 2016, **28**(21), 8016–8024, DOI: **10.1021/acs.chemmater.6b03761**.
20 Y. Zhong, *et al.*, Preferential Location of Dopants in the Amorphous Phase of Oriented Regioregular Poly(3-hexylthiophene-2,5-diyl) Films Helps Reach Charge Conductivities of 3000 S $cm^{-1}$, *Adv. Funct. Mater.*, 2022, **32**(30), 2202075, DOI: **10.1002/adfm.202202075**.

21 Y. Liu, *et al.*, High Polaron Yield p-Doping with an Ammoniumyl Radical Cation Oxidant for Organic Thin-Film Transistors, *ACS Appl. Electron. Mater.*, 2024, **6**(5), 3790–3800, DOI: 10.1021/acsaelm.4c00407.

22 M. Mirabedin, H. Vergnes, N. Caussé, C. Vahlas and B. Caussat, Liquid antimony pentachloride as oxidant for robust oxidative chemical vapor deposition of poly(3,4-ethylenedioxythiophene) films, *Appl. Surf. Sci.*, 2021, **554**, 149501, DOI: 10.1016/j.apsusc.2021.149501.

23 S. K. Mohapatra, *et al.*, Synthesis, characterization, and crystal structures of molybdenum complexes of unsymmetrical electron-poor dithiolene ligands, *Polyhedron*, 2016, **116**, 88–95, DOI: 10.1016/j.poly.2016.04.025.

24 R. Tiwari, E. Sonker, D. Kumar, K. Kumar, P. Adhikary and S. Krishnamoorthi, Preparation, characterization and electrical properties of alkali metal ions doped co-polymers based on TBF, *Mater. Sci. Eng., B*, 2020, **262**, 114687, DOI: 10.1016/j.mseb.2020.114687.

25 Y. P. Wang, *et al.*, Investigation of electron transport properties in $Li_2CO_3$-doped $Bepp_2$ thin films, *Org. Electron.*, 2015, **26**, 86–91, DOI: 10.1016/j.orgel.2015.07.023.

26 Z. Bin, L. Duan and Y. Qiu, Air Stable Organic Salt As an n-Type Dopant for Efficient and Stable Organic Light-Emitting Diodes, *ACS Appl. Mater. Interfaces*, 2015, **7**(12), 6444–6450, DOI: 10.1021/acsami.5b00839.

27 G. Chen, F. Liu, Z. Ling, P. Zhang, B. Wei and W. Zhu, Efficient Organic Light Emitting Diodes Using Solution-Processed Alkali Metal Carbonate Doped ZnO as Electron Injection Layer, *Front. Chem.*, 2019, **7**, 226, DOI: 10.3389/fchem.2019.00226.

28 S. D. Ha, J. Meyer and A. Kahn, Molecular-scale properties of $MoO_3$ -doped pentacene, *Phys. Rev. B: Condens. Matter Mater. Phys.*, 2010, **82**(15), 155434, DOI: 10.1103/PhysRevB.82.155434.

29 J. Meyer, R. Khalandovsky, P. Görrn and A. Kahn, $MoO_3$ Films Spin-Coated from a Nanoparticle Suspension for Efficient Hole-Injection in Organic Electronics, *Adv. Mater.*, 2011, **23**(1), 70–73, DOI: 10.1002/adma.201003065.

30 O. Yildiz, *et al.*, Optimized Charge Transport in Molecular Semiconductors by Control of Fluid Dynamics and Crystallization in Meniscus-Guided Coating, *Adv. Funct. Mater.*, 2022, **32**(2), 2107976, DOI: 10.1002/adfm.202107976.

31 Y. Jeon, Y. J. Shin, Y. Jeon and H. Yoo, Investigating the doping effect of molybdenum oxide on a p-type organic thin-film transistor and their application to unipolar circuits, *Org. Electron.*, 2023, **122**, 106914, DOI: 10.1016/j.orgel.2023.106914.

32 W. Wang, J. Han, J. Ying and W. Xie, $MoO_3$ Modification Layer to Enhance Performance of Pentacene-OTFTs With Various Low-Cost Metals as Source/Drain Electrodes, *IEEE Trans. Electron Devices*, 2014, **61**(10), 3507–3512, DOI: 10.1109/TED.2014.2346894.

33 R. Zhao, Y. Gao, Z. Guo, Y. Su and X. Wang, Interface Energy Alignment of Atomic-Layer-Deposited $VO_x$ on Pentacene: an in Situ Photoelectron Spectroscopy Investigation, *ACS Appl. Mater. Interfaces*, 2017, **9**(2), 1885–1890, DOI: 10.1021/acsami.6b12832.

34 Z. Yun, S. Li and S. Chen, Improving the Performance of Organic Field-Effect Transistors by Using $WO_3$ Buffer Layer, in 2019 IEEE International Conference on Electron Devices and Solid-State Circuits (EDSSC), Xi'an, China: IEEE, Jun. 2019, 1–3. doi: 10.1109/EDSSC.2019.8754129.

35 Y. Gao, *et al.*, Efficient Charge Injection in Organic Field-Effect Transistors Enabled by Low-Temperature Atomic Layer Deposition of Ultrathin $VO_x$ Interlayer, *Adv. Funct. Mater.*, 2016, **26**(25), 4456–4463, DOI: 10.1002/adfm.201600482.

36 C. Liu, X. Liu, T. Minari, M. Kanehara and Y.-Y. Noh, Organic thin-film transistors with over 10 $cm^2\ V^{-1}\ s^{-1}$ mobility through low-temperature solution coating, *J. Inf. Disp.*, 2018, **19**(2), 71–80, DOI: 10.1080/15980316.2018.1430068.

37 M. Ba, M. Erouel, S. Mansouri, L. Chouiref, M. Jdir and L. El Mir, Channel length effect of P3HT:ZnO hybrid blend layer on electrical characteristics of thin-film transistors, *Sens. Actuators, A*, 2023, **359**, 114470, DOI: 10.1016/j.sna.2023.114470.

38 Y.-H. Lin, *et al.*, Hybrid organic–metal oxide multilayer channel transistors with high operational stability, *Nat. Electron.*, 2019, **2**(12), 587–595, DOI: 10.1038/s41928-019-0342-y.

39 G. Nie, *et al.*, Mechanistic Analysis of Embedded Copper Oxide in Organic Thin-Film Transistors with Controllable Threshold Voltage, *ACS Omega*, 2019, **4**(5), 8506–8511, DOI: 10.1021/acsomega.8b02726.

40 G. Nie, J. Peng, L. Lan, R. Xu, J. Zou and Y. Cao, Tuning on threshold voltage of organic field-effect transistor with a copper oxide layer, *Org. Electron.*, 2011, **12**(3), 429–434, DOI: 10.1016/j.orgel.2010.12.012.

41 D.-J. Yun, S.-H. Lim, S.-H. Cho, B.-S. Kim and S.-W. Rhee, Effect of Cu, CuO, and Cu–CuO Bilayer Source/Drain Electrodes on the Performance of the Pentacene Thin-Film Transistor, *J. Electrochem. Soc.*, 2009, **156**(8), H634, DOI: 10.1149/1.3147264.

42 S.-J. Yoo, J.-H. Lee, J.-H. Lee and J.-J. Kim, Doping-concentration-dependent hole mobility in a $ReO_3$ doped organic semiconductor of 4,4′,4″-tris(*N*-(2-naphthyl)-*N*-phenyl-amino)-triphenylamine, *Appl. Phys. Lett.*, 2013, **102**(18), 183301, DOI: 10.1063/1.4804141.

43 E.-Y. Shin, J.-H. Lee, Y. Choi and M.-H. Kim, Enhanced charge injection in 6,13-bis(triisopropylsilylethylnyl)-pentacene field-effect transistors with a rhenium oxide buffer layer, *Semicond. Sci. Technol.*, 2019, **34**(3), 035008, DOI: 10.1088/1361-6641/aaff37.

44 Y. Jia, *et al.*, Low-Temperature Evaporable $Re_2O_7$: An Efficient p-Dopant for OLEDs, *J. Phys. Chem. C*, 2013, **117**(27), 13763–13769, DOI: 10.1021/jp400003m.

45 W. He, *et al.*, Surface Modification on Solution Processable $ZrO_2$ High-*k* Dielectrics for Low Voltage Operations of Organic Thin Film Transistors, *J. Phys. Chem. C*, 2016, **120**(18), 9949–9957, DOI: 10.1021/acs.jpcc.6b03638.

46 K. Tetzner, K. A. Schroder and K. Bock, Photonic curing of sol–gel derived HfO2 dielectrics for organic field-effect

transistors, *Ceram. Int.*, 2014, **40**(10), 15753–15761, DOI: 10.1016/j.ceramint.2014.07.099.

47 M. Geiger, *et al.*, Optimizing the plasma oxidation of aluminum gate electrodes for ultrathin gate oxides in organic transistors, *Sci. Rep.*, 2021, **11**(1), 6382, DOI: 10.1038/s41598-021-85517-7.

48 Y. X. Ma, W. M. Tang and P. T. Lai, Improved carrier mobility of pentacene organic TFTs by suppressed oxide growth at remote interface using nitrogen doping in high-k NdNbO dielectric, *Org. Electron.*, 2022, **102**, 106427, DOI: 10.1016/j.orgel.2021.106427.

49 S. Khound, J. K. Sarmah and R. Sarma, Hybrid $La_2O_3$-cPVP Dielectric for Organic Thin Film Transistor Applications, *ECS J. Solid State Sci. Technol.*, 2022, **11**(1), 013007, DOI: 10.1149/2162-8777/ac4a7e.

50 Y. Choi and C. K. Song, Low leakage current through zirconium oxide gate fabricated by low temperature solution process in OTFTs on plastic substrate, *Org. Electron.*, 2018, **52**, 195–199, DOI: 10.1016/j.orgel.2017.10.030.

51 Y.-Y. Yu, T.-J. Huang, W.-Y. Lee, Y.-C. Chen and C.-C. Kuo, Highly transparent polyimide/nanocrystalline-zirconium dioxide hybrid materials for organic thin film transistor applications, *Org. Electron.*, 2017, **48**, 19–28, DOI: 10.1016/j.orgel.2017.05.036.

52 F. Talalaev, *et al.*, High-Performance Organic Field-Effect Transistors Using Rare Earth Metal Oxides as Dielectrics, *ACS Appl. Electron. Mater.*, 2023, **5**(4), 2000–2006, DOI: 10.1021/acsaelm.2c01334.

53 Z. B. Wang, M. G. Helander, M. T. Greiner, J. Qiu and Z. H. Lu, Analysis of charge-injection characteristics at electrode-organic interfaces: Case study of transition-metal oxides, *Phys. Rev. B: Condens. Matter Mater. Phys.*, 2009, **80**(23), 235325, DOI: 10.1103/PhysRevB.80.235325.

54 M. G. Helander, Z. B. Wang, M. T. Greiner, J. Qiu and Z. H. Lu, Substrate dependent charge injection at the $V_2O_5$/organic interface, *Appl. Phys. Lett.*, 2009, **95**(8), 083301, DOI: 10.1063/1.3213553.

55 Y. Yi, *et al.*, The interface state assisted charge transport at the MoO3/metal interface, *J. Chem. Phys.*, 2009, **130**(9), 094704, DOI: 10.1063/1.3077289.

56 J. Meyer and A. L. Kahn, Electronic structure of molybdenum-oxide films and associated charge injection mechanisms in organic devices, *J. Photonics Energy*, 2011, **1**(1), 011109, DOI: 10.1117/1.3555081.

57 M. Kano, T. Minari and K. Tsukagoshi, Improvement of subthreshold current transport by contact interface modification in p-type organic field-effect transistors, *Appl. Phys. Lett.*, 2009, **94**(14), 143304, DOI: 10.1063/1.3115826.

58 Y. Yun, *et al.*, Enhanced Performance of Thiophene-Rich Heteroacene, Dibenzothiopheno [6,5-*b*:6′,5′-*f*] Thieno[3,2-*b*]Thiophene Thin-Film Transistor With $MoO_x$ Hole Injection Layers, *IEEE Electron Device Lett.*, 2017, **38**(5), 649–652, DOI: 10.1109/LED.2017.2687941.

59 C. Liu, *et al.*, Universal diffusion-limited injection and the hook effect in organic thin-film transistors, *Sci. Rep.*, 2016, **6**(1), 29811, DOI: 10.1038/srep29811.

60 S.-J. Yoo, J.-H. Chang, J.-H. Lee, C.-K. Moon, C.-I. Wu and J.-J. Kim, Formation of perfect ohmic contact at indium tin oxide/*N*,*N*′-di(naphthalene-1-yl)-*N*,*N*′-diphenyl-benzidine interface using $ReO_3$, *Sci. Rep.*, 2014, **4**(1), 3902, DOI: 10.1038/srep03902.

61 S. Beck, D. Gerbert, T. Glaser and A. Pucci, Charge Transfer at Organic/Inorganic Interfaces and the Formation of Space Charge Regions Studied with Infrared Light, *J. Phys. Chem. C*, 2015, **119**(22), 12545–12550, DOI: 10.1021/acs.jpcc.5b04398.

62 Y. Zhao, *et al.*, Transition metal oxides on organic semiconductors, *Org. Electron.*, 2014, **15**(4), 871–877, DOI: 10.1016/j.orgel.2014.01.011.

63 R. T. White, E. S. Thibau and Z.-H. Lu, Interface Structure of MoO3 on Organic Semiconductors, *Sci. Rep.*, 2016, **6**(1), 21109, DOI: 10.1038/srep21109.

64 Z. Yang, *et al.*, Enhanced Organic Thin-Film Transistor Stability by Preventing MoO3 Diffusion with Metal/$MoO_3$/Organic Multilayered Interface Source–Drain Contact, *ACS Appl. Mater. Interfaces*, 2023, **15**(1), 1704–1717, DOI: 10.1021/acsami.2c18780.

65 H. Kim, *et al.*, Versatile hole injection of $VO_2$: Energy level alignment at *N*,*N*′-di(1-naphthyl)-*N*,*N*′-diphenyl-(1,1′-biphenyl)-4,4′-diamine/$VO_2$/fluorine-doped tin oxide, *Org. Electron.*, 2015, **16**, 133–138, DOI: 10.1016/j.orgel.2014.10.044.

66 Q. Yao, *et al.*, Achieving tunable work function in MoO*x* thin films: A key to low-cost, high-performance organic electronics, *Thin Solid Films*, 2025, **817**, 140659, DOI: 10.1016/j.tsf.2025.140659.

67 J. Park, *et al.*, Flexible and Transparent Organic Phototransistors on Biodegradable Cellulose Nanofibrillated Fiber Substrates, *Adv. Opt. Mater.*, 2018, **6**(9), 1701140, DOI: 10.1002/adom.201701140.

68 M. J. Jung, Y. Kim, K.-J. Baeg and E. K. Lee, Ultraviolet Photodetector Fabrication with Low-Power Dissipation Based on Organic Suboptimal Source-Gated Transistor Architecture and MoO3-Doped Pentacene, *Small*, 2025, **21**(2), 2408772, DOI: 10.1002/smll.202408772.

69 P. Yan, *et al.*, Observation of hole injection boost *via* two parallel paths in Pentacene thin-film transistors by employing Pentacene: 4,4″-tris(3-methylphenylphenylamino) triphenylamine: $MoO_3$ buffer layer, *APL Mater.*, 2014, **2**(11), 116103, DOI: 10.1063/1.4901123.

70 H. Wang, *et al.*, Near-infrared-II photodetection realized by introducing organic-inorganic charge-transfer-complex photosensitive material into pentacene phototransistor, *Org. Electron.*, 2020, **77**, 105500, DOI: 10.1016/j.orgel.2019.105500.

71 Y. Yin, *et al.*, Near-infrared-II balanced ambipolar phototransistors realized by the optimized planar-heterojunction channel layer and charge-transfer-complex photosensitive layer, *Results Phys.*, 2023, **48**, 106456, DOI: 10.1016/j.rinp.2023.106456.

72 J.-H. Lee, D.-S. Leem, H.-J. Kim and J.-J. Kim, Effectiveness of p-dopants in an organic hole transporting material, *Appl. Phys. Lett.*, 2009, **94**(12), 123306, DOI: 10.1063/1.3107267.

73 Y.-J. Lim, S.-H. Lee, J. Lee, A. Gasonoo and J.-H. Lee, Optical and electrical analysis in various organic-inorganic stacked structures, *Org. Electron.*, 2022, **104**, 106488, DOI: 10.1016/j.orgel.2022.106488.

74 C.-H. Kim, Bulk versus Contact Doping in Organic Semiconductors, *Micromachines*, 2021, **12**, 742, DOI: 10.3390/mi12070742.

75 S.-H. Lee, G. Huseynova, H.-K. Choi, Y.-J. Lim, J. Lee and J.-H. Lee, Analysis of charge transfer complex at the interface between organic and inorganic semiconductors, *Org. Electron.*, 2021, **88**, 106001, DOI: 10.1016/j.orgel.2020.106001.

76 C. Y. H. Chan, C. M. Chow and S. K. So, Using transistor technique to study the effects of transition metal oxide dopants on organic charge transporters, *Org. Electron.*, 2011, **12**(8), 1454–1458, DOI: 10.1016/j.orgel.2011.04.023.

77 B. Yedikardeş, *et al.*, Enhanced Electrical Properties of P3HT:$WO_3$ Hybrid Thin Film Transistors, *J. Electron. Mater.*, 2021, **50**(4), 2466–2475, DOI: 10.1007/s11664-021-08764-4.

78 H. Li, L. Duan, D. Zhang and Y. Qiu, Electric Field inside a Hole-Only Device and Insights into Space-Charge-Limited Current Measurement for Organic Semiconductors, *J. Phys. Chem. C*, 2014, **118**(19), 9990–9995, DOI: 10.1021/jp5035618.

79 H. Li, L. Duan and Y. Qiu, Mechanisms of Charge Transport in Transition Metal Oxide Doped Organic Semiconductors, *J. Phys. Chem. C*, 2014, **118**(51), 29636–29642, DOI: 10.1021/jp510575q.

80 C.-W. Chu, S.-H. Li, C.-W. Chen, V. Shrotriya and Y. Yang, High-performance organic thin-film transistors with metal oxide/metal bilayer electrode, *Appl. Phys. Lett.*, 2005, **87**(19), 193508, DOI: 10.1063/1.2126140.

81 M. Waqas Alam, Z. Wang, S. Naka and H. Okada, Mobility enhancement of top contact pentacene based organic thin film transistor with bi-layer GeO/Au electrodes, *Appl. Phys. Lett.*, 2013, **102**(6), 061105, DOI: 10.1063/1.4792235.

82 M. W. Alam, S. Wang, S. Naka and H. Okada, Top Contact Pentacene Based Organic Thin Film Transistor With Bi-layer $TiO_2$ Electrodes, *J. Photopolym. Sci. Technol.*, 2012, **25**(5), 659–664, DOI: 10.2494/photopolymer.25.659.

83 A. Ablat, A. Kyndiah, G. Houin, T. Y. Alic, L. Hirsch and M. Abbas, Role of Oxide/Metal Bilayer Electrodes in Solution Processed Organic Field Effect Transistors, *Sci. Rep.*, 2019, **9**(1), 6685, DOI: 10.1038/s41598-019-43237-z.

84 T. Borthakur and R. Sarma, Study of the Performance Enhancement of $MoO_3$/Au Bilayer Source–Drain Electrode for Top-Contact Pentacene-Based OTFT, *J. Electron. Mater.*, 2022, **51**(9), 5336–5342, DOI: 10.1007/s11664-022-09765-7.

85 T. Borthakur and R. Sarma, Effects of $V_2O_5$/Au bi-layer electrodes on the top contact Pentacene-based organic thin film transistors, *Indian J. Phys.*, 2017, **91**(5), 563–567, DOI: 10.1007/s12648-017-0956-8.

86 S. K. Jain, A. M. Joshi and L. R. Cenkeramaddi, Dielectric Modulated Bilayer Electrode Top Contact OTFT for Label Free Biosensing, *IEEE Access*, 2023, **11**, 23714–23725, DOI: 10.1109/ACCESS.2023.3253563.

87 H.-R. Byun and Y.-G. Ha, UV-Cured Hafnium Oxide-Based Gate Dielectrics for Low-Voltage Organic and Amorphous Oxide Thin-Film Transistors, *J. Nanosci. Nanotechnol.*, 2019, **19**(7), 4249–4253, DOI: 10.1166/jnn.2019.16329.

88 Y. Gong, *et al.*, Room Temperature Fabrication of High Quality $ZrO_2$ Dielectric Films for High Performance Flexible Organic Transistor Applications, *IEEE Electron Device Lett.*, 2018, **39**(2), 280–283, DOI: 10.1109/LED.2017.2783945.

89 K. Zhao, *et al.*, Room-Temperature Fabrication of High-Quality Lanthanum Oxide High-$\kappa$ Dielectric Films by a Solution Process for Low-Power Soft Electronics, *Adv. Electron. Mater.*, 2019, **5**(10), 1900427, DOI: 10.1002/aelm.201900427.

90 P. Dacha, *et al.*, Eco-Friendly Approach to Ultra-Thin Metal Oxides- Solution Sheared Aluminum Oxide for Half-Volt Operation of Organic Field-Effect Transistors, *Adv. Funct. Mater.*, 2024, **34**(41), 2315850, DOI: 10.1002/adfm.202315850.

91 P. Kumar, V. N. Mishra and R. Prakash, Ultralow-Voltage Eco-Friendly Water-Induced $LiO_x$/$AlO_x$ Bilayer Dielectric-Based OFET, *IEEE Trans. Electron Devices*, 2023, **70**(8), 4345–4350, DOI: 10.1109/TED.2023.3285172.

92 Q. H. Wang, Y. Heng Deng, H. Sun, J. Ping Xu and P. T. Lai, Hysteresis-Free High-Performance Pentacene Organic Thin-Film Transistor by Sputtering Amorphous Barium Titanate as Ultrathin High-k Gate Dielectric, *IEEE Trans. Electron Devices*, 2024, **71**(10), 6268–6274, DOI: 10.1109/TED.2024.3438069.

93 S. Mandal, *et al.*, Organic Field-Effect Transistor-Based Ultrafast, Flexible, Physiological-Temperature Sensors with Hexagonal Barium Titanate Nanocrystals in Amorphous Matrix as Sensing Material, *ACS Appl. Mater. Interfaces*, 2019, **11**(4), 4193–4202, DOI: 10.1021/acsami.8b19051.

94 G. Kim, C. Fuentes-Hernandez, X. Jia and B. Kippelen, Organic Thin-Film Transistors with a Bottom Bilayer Gate Dielectric Having a Low Operating Voltage and High Operational Stability, *ACS Appl. Electron. Mater.*, 2020, **2**(9), 2813–2818, DOI: 10.1021/acsaelm.0c00487.

95 S. Khound and R. Sarma, High Performance Organic Thin Film Transistors Using Pentacene-Based Rare-Earth Oxide Bilayer Gate Dielectric, *J. Electron. Mater.*, 2019, **48**(7), 4491–4497, DOI: 10.1007/s11664-019-07232-4.

96 K. Gallegos-Rosas, P. Myllymäki, M. Saarniheimo, S. Sneck, R. Raju and C. Soldano, Hafnium Aluminate–Polymer Bilayer Dielectrics for Organic Light-Emitting Transistors (OLETs), *ACS Appl. Electron. Mater.*, 2024, **6**(2), 1493–1503, DOI: 10.1021/acsaelm.3c01813.

97 S. Lakshmi Priya, T. Wei Haung, K. Agrahari and Y. Wu Wang, The comprehensive study of hybrid dielectric layer adopted organic thin film transistors for low voltage operation, *J. Mol. Liq.*, 2024, **409**, 125431, DOI: 10.1016/j.molliq.2024.125431.

98 H. N. Le, R. Wang, B. Hou, S. Kim and J. Kim, Preparation of Low-Temperature Solution-Processed High-$\kappa$ Gate Dielectrics Using Organic–Inorganic $TiO_2$ Hybrid Nanoparticles, *Nanomaterials*, 2024, **14**(6), 488, DOI: 10.3390/nano14060488.